An Overview of the Recent Advances in Inorganic Nanotubes

Marco Serra,[a] Raul Arenal * [b,c,d] and Reshef Tenne * [a]

Advanced nanomaterials play a prominent role in nanoscience and nanotechnology developments, opening new frontiers in these areas. Among these nanomaterials, inorganic nanotubes, due to their unique characteristics and enhanced chemical and physical properties, have been considered as one of the most interesting nanostructures. In recent years, important progresses have been achieved in the production and study of such nanomaterials, as boron nitride, transition metal dichalcogenide nanotubular structures, misfit based nanotubes and other hybrid/doped nanotubular objects. This review is devoted to the in-depth analysis of recently studies on the synthesis, atomic structure, properties and applications of inorganic nanotubes and related nanostructures. Particular attention is also paid to the growth mechanism of such nanomaterials. This is a crucial point for the challenges ahead related with their massive production of high-quality defect-free nanotubes for variety of applications.

Introduction

General

Inorganic compounds with layered structure (2D materials) are investigated for almost 100 years.[1-8] In the early years much of the research was dedicated to naturally occurring 2D materials, like molybdenite (MoS_2), chrysotile ($Mg_3Si_2O_5(OH)_4$), kaolinite ($Al_2Si_2O_5(OH)_4$), etc. Much of the early work from the end of WWII to the late 60's of the 20's century was summarized by Wilson and Yoffe.[9] Later-on the book series on layered compounds, edited by F. Levy summarized the updated knowledge in the sixties, seventies of the last century- see for example Ref. 10. In the early 80's Tributsch's discovery[11] of high efficiency and stable photoelectrochemical cells for the conversion of solar energy into electricity from WS_2 and MoS_2 and their respective selenides elicited much research on 2D-materials. Thus, photoelectrochemical and later-on also photovoltaic cells based on 2D-materials with solar to electrical conversion efficiency exceeding 10%[12] and subsequently >13%,[13] were reported. Concomitantly, the discovery of the so-called "charge density waves" phase in layered metal dichalcogenides, which was reviewed in,[14] led to much research on the structural and electrical properties at various temperatures. Intercalation of 2D-metal dichalcogenides was demonstrated as early as 1959.[15] Subsequently, superconductivity was discovered in pyridine intercalated TaS_2[16] and potassium intercalated MoS_2,[17] which prompted a lot of research. Later-on, the role of chemical and electrochemical intercalation of alkali metal ions in 2D-materials, like MoS_2[18] and in CoO_2[19] was recognized as an important route for the storage of electrical energy. These works heralded the extensive research in the field of intercalation batteries, which has greatly intensified in recent years. The outstanding catalytic reactivity of MoS_2 nanoparticles (NP) decorated by Co and Ni atoms for the mineralization of organo-sulfur (and organo-nitrogen) compounds[20] gave rise to a remarkable industrial application of this material for the removal of sulfur (and nitrogen) from gasoline, i.e. hydrodesulfurization.[21]

The first reports on the cleavage of MoS_2[3] and its exfoliation via Li intercalation followed by immersion in aqueous suspensions[22] commanded minor attention until the last decade. Alongside this research, Koma[23] demonstrated that in contrast to 3D materials, epitaxy of a few crystalline layers of 2D-materials can be achieved onto substrates lacking good lattice-match with the film. The advent of graphene research following the discovery of "massless" (Dirac) electrons,[24] incited an analogous research in exfoliated 2D-materials (sometimes called "beyond graphene" or "graphene related materials" (GRMs)). The realization of the first high-performance transistor based on a single layer MoS_2[25] and the observation of direct electronic transition and strong luminescence in MoS_2 monolayer[26] elicited a new wave of interest in 2D-materials and tense research effort in different directions and for different applications of 2D-materials. Encapsulating the MoS_2 layer by BN monolayer was found to have remarkable effect on the field effect mobility of the charge carriers,[27] making it the standard methodology for preparation of field effect transistors and other devices based on 2D monolayers.

Pauling, who took great interest in 2D-materials early in his career, was the first to elucidate the structure of MoS_2.[3] Later-on he studied naturally occurring layered alumina (magnesia) silicates and offered the first mechanism for the formation of nanotubes from 2D-materials.[5] He discriminated between naturally-occurring layered compounds with asymmetric structure, such as halloysite (hydrated form of kaolinite-$Al_2Si_2O_5(OH)_4 \cdot 2H_2O$), and chrysotile to those with symmetric structure, like brucite, mica and molybdenite (see **Fig. 1**). In the
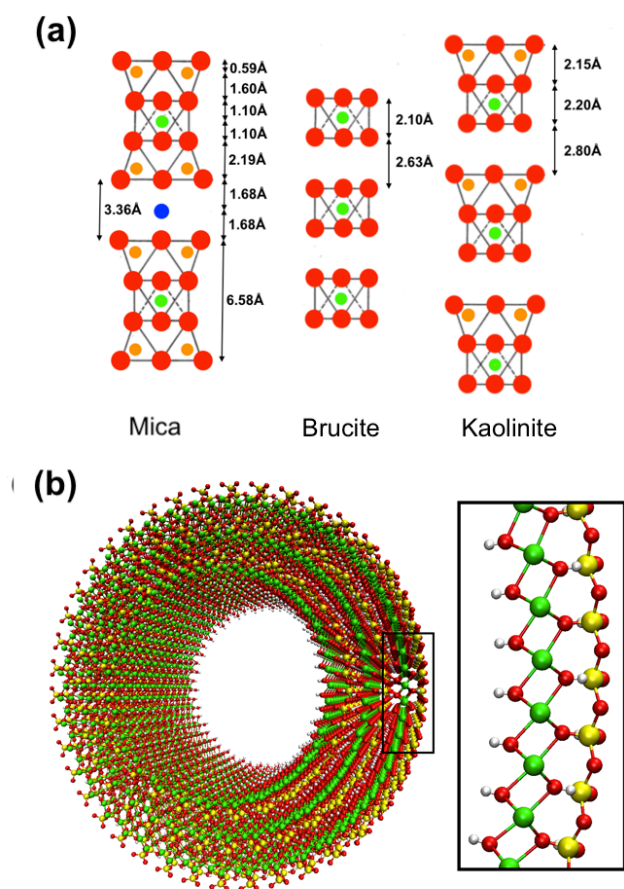
Figure 1 (a) Schematic rendition of the layered chlorites (alumosilicates); (b) Drawing of halloysite nanotubes (courtesy of Dr. A.N. Enyashin).

Fig. 2 shows a schematic drawing of the (001) plane of graphene (**a**) and MoS_2 (**b**). Whilst the bulk atoms are fully bonded, the rim atoms possess dangling bonds and promote folding of the slabs and their seaming into nanotubes.
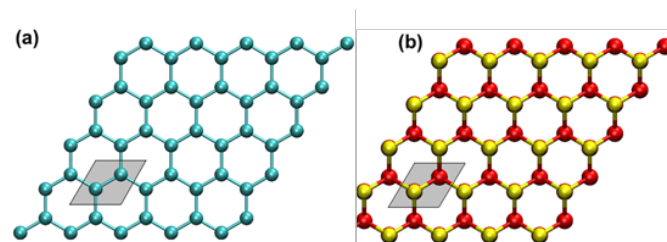

Figure 2 Drawing of the graphene (a) and MoS_2 (b) lattices, emphasizing the different chemical bonding (coordination) of the bulk and rim atoms.

Typical scanning (SEM) and transmission electron microscopy (TEM) images are shown in **Fig. 3**, displaying a multiwall fullerene-like nanoparticle of MoS_2 (IF-MoS_2) (**a**) and WS_2 nanotubes (INT-WS_2) (**b**) and (**c**). These pictures represent the most generic forms of the hollow closed-cage structures, so typical for nanoparticles of 2D compounds. Over the years since its discovery, these generic nanostructures have been synthesized from numerous 2D compounds. Furthermore, many theoretical works and computer calculations were dedicated to elucidating the structure and properties of nanotubular structures from 2D-compounds.[35]
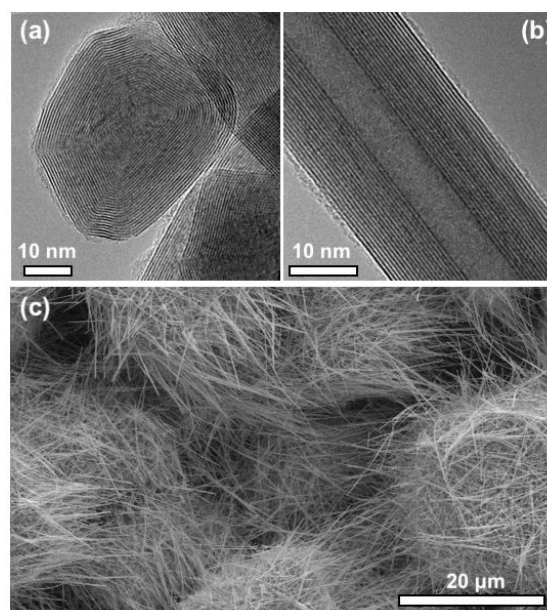
asymmetric ones, the *a-b* plane (0001) of the alumina octahedra side are larger than the counter side of the silica tetrahedra. Consequently, the alumosilicate layer afford a large bending strain and eventually could form a rolled-up structure, namely-nanotubes (NT). It took another twenty years for transmission electron microscopes to gain sufficient resolution in the early 50's of the last century, and thus observe chrysotile nanotubes, directly. [28,29] With the same reasoning in mind, he suggested that layered compounds with symmetric unit cell along the *c*-axis, like brucite, mica and also molybdenite suffer no lattice strain and consequently have no driving force towards folding and eventually forming nanotubular structure (see **Fig. 1a**). However, with the advent of C_{60}[30] and carbon nanotubes[31] research, a new paradigm for the formation of nanotubes and fullerene-like structures from 2D materials emerged.[32-34] The stimulus for the formation of such hollow closed structures are the reactive metal and non-metal rim atoms, which are only partially bonded. Energetically, it pays the nanolayers of the 2D material to fold into a closed seamless structure, which more than compensates for the elastic energy of folding.

Figure 3. (a) TEM image of IF-MoS_2 nanoparticle; (b) TEM image of WS_2 nanotube; (c) SEM micrograph of WS_2 nanotubes powder.

Inorganic fullerene-like nanoparticles (IF) and nanotubes (INT) of MoS_2 and in particular WS_2 are now synthesized in substantial quantities as pure phases. They were shown to be absolutely stable only in the nano-size regime. The high-temperature

reactions (800-950 °C) leading to these nanostructures are difficult to control, in particular under mass production conditions. However, once the early difficulties waned and they became available in sizeable amounts, these phases could be characterized by many techniques and delineated from their bulk platelet structure. These analyses provided a distinct fingerprint to these nanophases through mechanical,[36-38] electrical[39,40] and optical[41,42] measurements, distinguishing them clearly from the bulk phase. Unfortunately, the large bending energy involved in the formation of such nanostructures can be only compensated by having multiple layers, which favors multiwall INT (IF) rather than single wall nanostructures.[43]

Early on, it was hypothesized and later realized that these nanoparticles could serve as superior solid lubricants.[44,45] Following many years of research&development, various lubricating and metal working fluids incorporating IF-WS_2 nanoparticles have been manufactured and commercialized and their market share is expanding rapidly in recent times. Other products, under intensive development are polymer-based nanocomposites, for diverse applications, including medical technologies, shock-resistant fabrics, and a lot more. Two important aspects of these nanoparticles which make them particularly amenable for large scale applications is their facile dispersion into different matrices and biocompatibility and low toxicity.[46]

Nanotubes from misfit layered compounds

Recognizing the difficulties to synthesize nanotubes from binary 2D materials, a guiding principle for the synthesis of nanotubes exploiting the richness of the chemistry of 2D materials from ternary and quaternary compounds was searched. Among these ternary compounds, "misfit" layered compounds (MLCs) stand-out for their (relative) stability and propensity to form hollow closed-cage nanostructures. In fact ternary layered materials, such as $PbTiS_3$[47] and $PbNbS_3$[48] were reported early on, but their misfit (non-stoichiometric composition) was not appreciated. Chalcogenide-based misfit layered compounds (MLC) of the form $(MX)_{1+x}(TX_2)_m$ (with M = Sn, Pb, Sb, Bi, rare earth atom (Ln); T = Sn, Ti, V, Cr, Nb, Ta; X = S, Se, Te; 0.08 < x <0.32; m = 1,2,3) have a planar composite structure, composed of two alternating layers, namely, MX and TX_2 (see **Fig. 4**), hereafter referred to as MX-TX_2.

The alternating layers of the two subsystems are stacked along the common *c*-axis forming a superstructure. The MX slab has a distorted rocksalt structure consisting of a two-atom-thick {001} slice of the MX lattice. The pseudo-hexagonal TX_2 layer consists of a three-atom-thick sandwich structure. Here, the transition metal T is surrounded by six chalcogen atoms, in either an octahedral (T = Sn, Ti, V, Cr) or trigonal prismatic coordination (T = Nb, Ta). The MLC lattice is lacking a periodicity along at least one-direction (usually the *a*-axis) leading to incommensurate

structural modulation.[49,50] Note that, as the number of atoms in any inner layer is smaller than that of an adjacent outer one, multiwall nanotubes of any 2D material are incommensurate. Clues to the existence of tubular structures from MLC were available,[51-53] but not in the range sizes of nanomaterials, and then, no systematic investigation of these nanostructures was undertaken until recently.
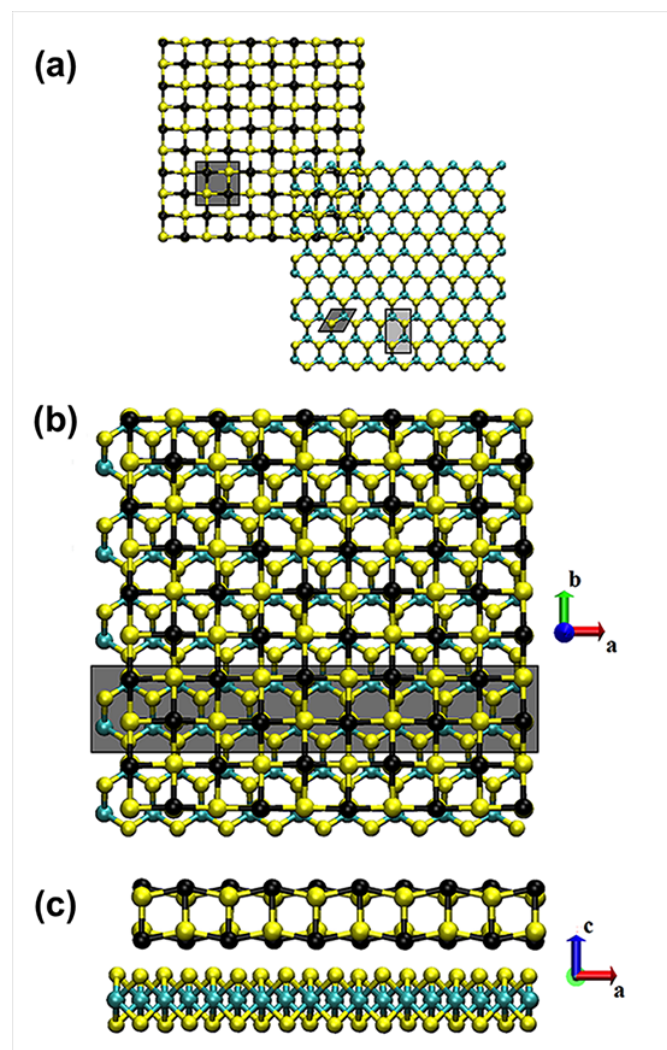

Figure 4. Illustration of the two sublattices composing the misfit layered compounds structure. (a) The two separate sublattices and their respective unit cell. Projection of the MLC lattice along the *a*-axis (b) and the *c*-axis (c).

Combining the built-in asymmetry along the *c*-axis of "misfit" layered compounds (the Pauling's mechanism) and fine-tuning the reaction conditions to allow seaming of the edges in 2D nanocrystals (annotated the Kroto-Iijima-Tenne's mechanism), provided a powerful synthetic approach for obtaining nanotubes (nanoscrolls) from numerous MLCs in recent years.[54-56] **Fig. 5a** shows a SEM micrograph of an assortment of LaS-TaS_2 nanotubes. **Fig. 5b** shows a TEM image of an ErS-TaS_2 nanotube with intensity profile (Fig. 5c), from which the interlayer spacing is calculated.
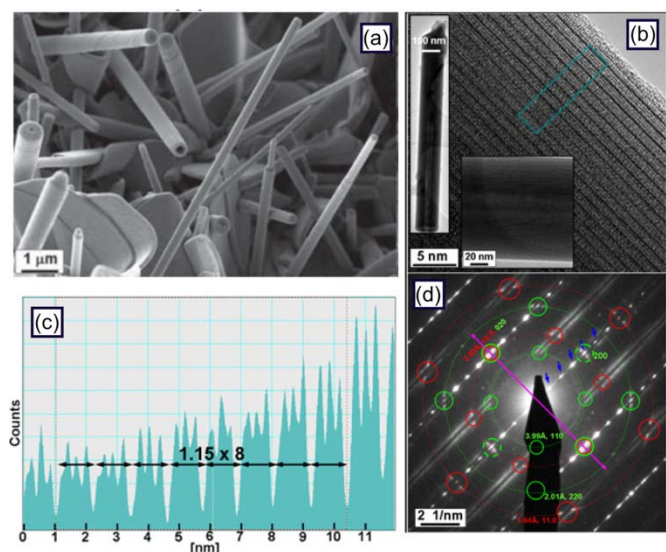
Figure 5. SEM and TEM analyses of LaS-TaS₂ nanotubes: (a) SEM image of an assortment of nanotubes; (b) TEM images of such nanotubes in different magnifications; (c) intensity profile of the signal obtained from the cyan rectangle in (b); (d) electron diffraction pattern obtained from the nanotubes. Adapted from Ref. 120 with permission of the RSC.

The electron diffraction pattern (EDP) shows that the growth direction of the nanotube (purple arrow) coincides with the common *b*-axis of the lattice, i.e. the [10.0] axis of the TaS₂ and the [020] axis of the LaS. Consequently, the diffraction of the (110) plane (and its multiple- (220)) of the LaS (green) makes 45° with respect to the growth direction of the nanotube and the (incommensurate) *a*-plane (200) and (11.0) of the LaS and TaS₂, respectively, diffract at 90° with respect to the growth direction. The diffraction spots of the *c*-axis are marked by blue arrows. The chirality of the tubes (about 3°) can be calculated from the (half) arc of the splitted diffraction spots.
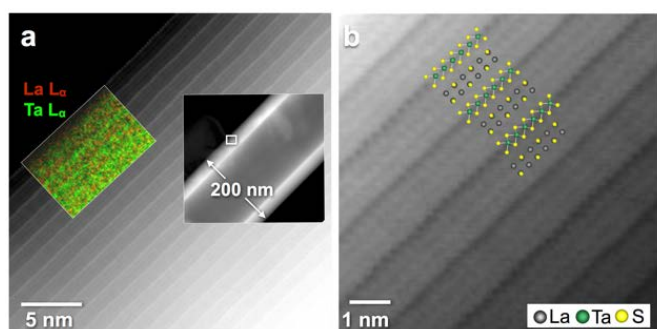

Figure 6. High-resolution STEM images of a LaS-TaS₂ nanotube. (a) HAADF image. The insets show an HAADF image corresponding to a larger field of view, with a marker indicating the magnified region, and a high-resolution chemical map acquired by EDS. (b) Atomic-resolution BF STEM image, with the overlaid structure projections of the LaS and TaS₂ layers. Adapted from Ref. 120 with permission of the RSC.

Fig. 6a shows an aberration-corrected high-angle annular dark-field (HAADF)-scanning transmission electron microscope (STEM) image of a LaS-TaS₂ nanotube with energy dispersive X-ray spectroscopy (EDS) chemical maps of Ta and La overlaid on the lattice image of the nanotube. **Fig. 6b** shows the high-resolution image of this nanotube with the calculated lattice structure overlaid on the TEM image. Thus, the chemical and structural richness of quasi-1D nanostructures from MLC; their heavy atoms with many electrons each and their chirality, offer research opportunities into intriguing multi-electron collective phenomena at low temperatures.

Other Inorganic Nanotubes

From the 50s and 70s of 20th century, other tubular nanostructures based on clay minerals as the halloysite and imogolite forms have been investigated.[57-67] The atomic configuration of both systems is very different even if both of them are based, at least in the most standard or usual forms, on layered aluminosilicate materials. Indeed, in the case of Imogolite NTs, the (Al(OH)₃) layer forms the external surface of the tubular structure and the Si-O based groups (siloxane groups) the internal one. In the halloysite NTs, it is the opposite, with the Si-O based groups (silanol groups) forming the outer layer of these NTs. The length of these NTs can be up to a few microns and they can be found forming single-layer NTs with a diameter of less than 2 nm. In addition, at least for the imogolite system, their internal surface can be modified via different procedures as for instance by replacing the Si atoms with Ge, forming new tubular structures composed of 1 or 2 layers or even via the functionalization with organic moieties. All these systems possess very interesting properties, which, due to all these potential modifications, can be tuned. Thus, they are very attractive for industrial applications in catalysis as well as for gas separation and capture, controlled drug delivery, composites, and more.

In what follows, a detailed account of the recent developments in the field of inorganic nanotubes and also fullerene-like nanoparticles is described with emphasis on the relationships between the materials chemistry- synthesis, structure and properties. Some recent developments in the applications of such nanoparticles are discussed in brief as well at the end of this review.

Synthesis

The driving force for the formation of most inorganic nanotubes (INT) as well as inorganic fullerene-like (IF) nanoparticles lies in the intrinsic instability of nascent two-dimensional crystalline layered compounds in the planar form. The healing of the dandling bonds of the peripheral atoms is considered as the main energetic stimulus, which can overcome the elastic strain associated with the bending of the layers and drive the reaction towards seaming of the layers. These considerations are

particularly meaningful in the case of crystalline layers of reduced (nano) dimensions, in which the dangling bonds of the rim atoms constitute a major part of the total number of atoms in the slab. Therefore, IF/INT become stable only in the nano-range, i.e. below about 200 nm in diameter.

The chemical synthesis of IF/INT, regardless of the precise chemical composition of the 2D material and excluding several specific examples (*vide infra*), involves high temperature reactions, which is a prerequisite for softening of the 2D layers and increasing their structural fluctuations. Thus, the high temperatures enhance the probability of folding and seaming of the 2D layers and the genesis of the hollow closed IF/INT. These reactions require precise control over the different parameters in order to govern the diffusion and nucleation rates. This point represents a notable difficulty from the experimental point of view. Furthermore, the synthesis of each kind of IF or INT is done via a specific chemical route. This diversity necessitates using a rich chemical vocabulary for the solid-state synthesis. In the following, a few recent developments in the synthesis of nanotubes and fullerene-like nanoparticles from 2D-mateials will be described.

Nanotubes from binary 2D compounds

Several unique strategies have been developed to synthesize nanotubes in recent years. They will be briefly described.

Templating

Templating, i.e. using existing nanotubes, like those from carbon, BN or WS_2, which are available in sizeable amounts, can greatly facilitate the growth of new (core-shell) nanotubes from 2D materials, a few recent examples to this effect will be demonstrated below.

The synthesis of core-shell $PbI_2@WS_2$ nanotubes,[68] presented a new templating strategy for obtaining INT from layered metal halides, which are otherwise difficult to produce. The incipient 2D clusters, which form either within the hollow core on the inner surface or the outer nanotube perimeter, are forced to fold and eventually seam into core-shell nanotubular structures. In a follow-up work the synthesis of $BiI_3@WS_2$ and $SbI_3@WS_2$ nanotubes were reported.[69] Model calculations revealed that the core-shell nanotubular structures are limited to a hollow core of an 8 nm diameter. The excessive elastic strain prevented wetting and folding of the bulky layered metal-iodides within a core size below 6-8 nm in diameter, eliciting the formation of BiI_3 nanowires, rather than nanotubes, within WS_2 nanotubes with smaller core.

The templating strategy is particularly useful for the synthesis of nanotubes from layered metal-halides, which possess relatively low melting point and are highly hygroscopic and consequently difficult to work with. In one recent work, single-wall nanotubes of the layered compounds CeI_3, $CeCl_3$, $TbCl_3$ and ZnI_2 were obtained by template-assisted high-temperature growth using multiwall carbon nanotubes (MWCNTs) as directing agents (see **Fig. 7 (a-b)**).[68,70-72] This solvent-free high temperature approach was based on the use of the inner cavities of CNTs as hosting templates. Thus, the growth of lead diiodide single wall nanotubes (SWNTs), with diameters ranging from 3.5 to 7.5 nm, as well as nanowires, were reported, see **Fig. 7 (c-h)**.[70]
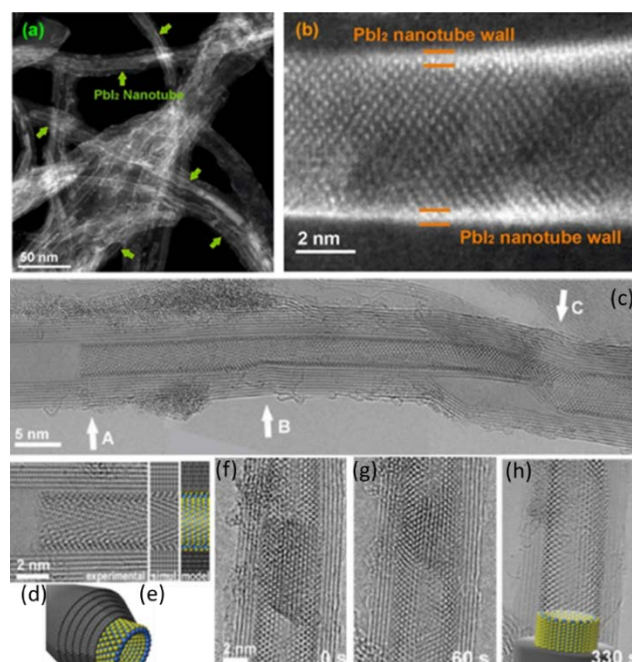

Figure 7. HAADF-STEM images of $PbI_2@MWCNTs$ prepared by laser irradiation. (a) HAADF-STEM image (as prepared), (b) high resolution aberration corrected HAADF-STEM image. Green arrows in panel (a) point to well-defined single-walled inorganic PbI_2 nanotubes, while orange lines in panel b indicate the PbI_2 nanotube wall (adapted from Ref. 68 with permission of the ACS publishing). (c)-(d) HRTEM image of a single-walled PbI_2 NT. b) Detail of the HRTEM image (area A) with its corresponding simulation and model (cross section along the main axis). (e) Schematic representation of the grown PbI_2 SWNTs (cyan and green spheres representing Pb and I atoms, respectively) within the inner cavities of MWCNTs (grey spheres). (f)-(h) Series of images showing the transformation from a nanorod fragment onto a SWNT via electron beam radiation. A sketch is included in the last image. (Adapted from Ref. 70 with permission of Wiley).

In a related work this group has laser ablated PbI_2 (and ZnI_2) in the presence of CNT mesh, obtaining core-shell single wall $PbI_2@CNT$ nanostructures in high yields.[72] Similarly,[73] a complex series of core-shell nanostructures were obtained by annealing layered GdI_3 in the presence of CNT mesh. In the case of double wall CNT with open end and hollow core of only 0.3 nm, pure iodine nanowires were encapsulated. On the other hand, Gd nanowires were encapsulated in triple wall CNT with a hollow core 1.5 nm in diameter. However, for triple wall CNT with larger opening, GdI_3 nanowires and nanotubes were found to crystallize within the hollow core.

Using CNT as a template, the synthesis of core-shell $CNT@MoS_2$ nanotubes was pursued intensively in recent years,[74] especially

in relation to the search for anode material for Li-ion batteries[75] and for the catalytic production of hydrogen.[76] In this case, the outer MoS_2 nanotubes provide the specific functionality, i.e. catalytic reactivity or lithium intercalation, while the inner carbon nanotubes endow the electrical conductivity required to shunt the electrical charges toward the current collector. Furthermore, few layers molybdenum trioxide nanotubes were obtained using CNT as a template.[77] Another promising strategy involved the anodization of Mo foil, which resulted in an array of MoO_{3-x} nanotubes. Subsequently, this template was sulfidized and a network of MoS_2 nanotubes was obtained. This hierarchical structure exhibited sizeable capacity towards electrochemical lithium uptake and for catalytic generation of hydrogen under acidic conditions.[78]

Single-walled boron nitride nanotubes (SW-BNNTs) have been produced inside SW carbon NTs, via a nano-templating reaction, employing ammonia borane complexes as precursors at temperatures close to 1400 °C.[79] These NTs displayed a narrow diameter distribution of 0.7 ± 0.1 nm.

Related to these works, several interesting studies have been developed using BNNTs as templates for growing nanostructures inside their hollow core.[80-86] For instance, amorphous carbonaceous structures have been crystallized forming carbon NTs via a catalyst-free procedure, at room temperature and electron beam irradiation, see Fig. 8 (a)-(b).[83] In another work, single wall BNNT with the smallest known radius (0.45 nm) with armchair (3,3) configuration where obtained *in-situ* by irradiating BN bilayer with electron beam of the TEM.[87] These last experiments as well as previous developments over the last 15 years are a powerful manifestation of an electron beam induced materials engineering.[81,83] It is worth mentioning that the world's smallest coaxial cable has been obtained following a complementary approach based on thermal treatments (1200 °C) in argon atmosphere of BNNTS filled with fullerenes. Under these thermal treatments the fullerenes were transformed into CNTs of 0.9 nm in diameter, forming again these interesting and attractive hybrid nanostructures.[86]

In another series of works a universal and facile wet-chemistry method was used for metal filling of BNNTs, see Fig. 8 (c-g).[85]
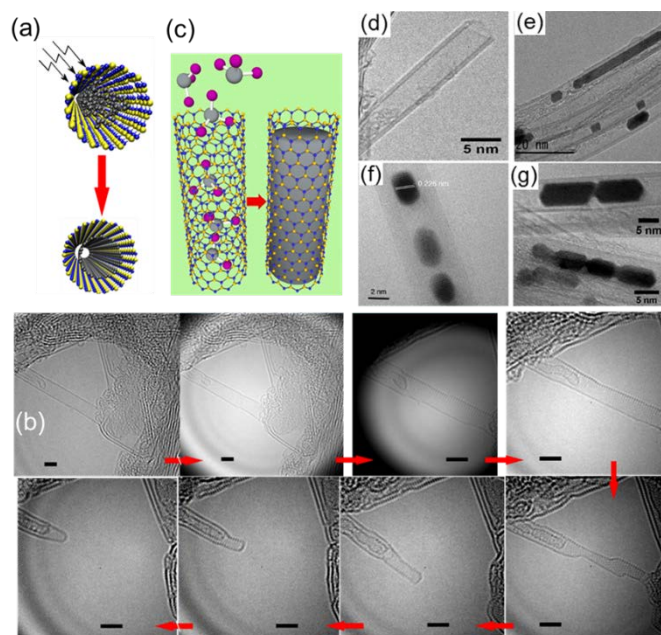

Figure 8. (a) Schematic representation showing the transformation via electron irradiation of a SWBNNT containing disordered carbon and its transformation to concentric hybrids BN@C SW-NTs. (b) Eight-frame HRTEM image sequence displaying the formation process of a crystalline CNT from amorphous C encapsulated in a BNNT under electron beam irradiation (high doses for short periods of time). Scale bars in Fig. 8 (b) are 2 nm. (Adapted from Ref. 83 with permission of the ACS publishing). (c) Sketch showing the wet-chemistry method for efficient metal filling of BNNTs. (d-g) HRTEM micrographs of: a double-wall BNNT with opened tip after nitric acid treatment; encapsulated Pt nanostructures within BNNTs; Pt nanoparticles and nanosausage formed by sintering of Pt nanoparticles. (Adapted from Ref. 85 with permission of the ACS publishing)

Catalytic growth

The first catalytically-induced growth of INT was demonstrated in the case of SnS_2 tubes using Bi as a catalyst.[88] The synthesis of MoS_2, $MoSe_2$, WS_2, WSe_2 nanotubes via solar ablation using Pb as a catalyst was also confirmed.[89] Here, highly concentrated beam of sunlight was focused on a quartz ampoule filled with a precursor mixture containing metals and metal sulphides (or selenides) in the presence of graphite or active carbon. The carbon powder served as an absorbing media for the solar light, which led to the fast heating of the ampoule content to temperatures exceeding 2000 °C within a minute or two. The three-step reaction mechanism commenced with conversion of the MX_2 (M=Mo, W; X=S, Se) powder into metal oxide via reaction with the residual oxygen and water vapour in the ampoule; subsequently, promoted by the lead atoms, the oxide nanoparticles grew into nanowhiskers, and where finally back-converted into MX_2 nanotubes using the well investigated reaction with sulphur (selenium) vapour. Unfortunately, this catalytic reaction could not be harnessed at temperatures below 1000 °C, which would allow scaling-up of the nanotubes'

syntheses. However, recently MoS$_2$ nanotubes were synthesized by chemical vapour deposition using FeO nanoparticles as catalyst.[90]

GaS nanotubes were also synthesized by solar ablation in the presence of lead as growth promoter.[91] Liquid gallium and lead are miscible at temperatures above 600 °C, but upon cooling they segregate into Ga-rich and Pb-rich phases. Once the lead-rich phase solidified in a cylindrical rod-shape (around 300 °C), the gallium-rich phase reacted with the sulphur vapour forming the cylindrical contour of the GaS nanotube engulfing the Ga nanowire.

Doping

Doping is an old and effective strategy for modifying and controlling the electrical, optoelectronic, catalytic and other properties of semiconductor matrices by adding minute amounts of foreign atoms into substitutional or interstitial site of the host lattice. One of the most demanding tasks in this process, is controlling the position and concentration of the guest atoms incorporated into the host lattice. In general, controlling the position of the Fermi level in the semiconductor matrix requires dopant concentrations below 1000 ppm (<0.1 at. %). Analysis of such small quantities of the dopant atoms invoked a dilemma, since analytical techniques, such as X-ray diffraction (XRD), spectroscopy (XPS), Auger spectroscopy and others, are not sufficiently sensitive for concentrations below 0.5 at% and their accuracy is hampered by the low signal to noise ratio. TEM, and in particular, spatially-resolved electron energy loss spectroscopy (SR-EELS) is one of the most appropriate techniques for analysing in great detail such nanomaterials.[80,92-95] Recently, the syntheses of MoS$_2$ nanoparticles with fullerene-like structure doped with small amounts (<500 ppm) of Re[96] and Nb[97] atoms, were reported. Being substitutional to Mo atoms in the lattice and having one extra (less) electron, the dopant Re (Nb) atoms impose *n*-type (negative surface charge) and *p*-type behaviour (positive surface charge) on the IF-MoS$_2$ NP, respectively. The extra charge induced by the dopant atoms combines (Re) and compensates (Nb) the native negative charge acquired by the sulphur vacancies. Due to their surface charge, the Re-doped NP were shown to self-repel each other forming stable suspensions and led also to very low friction coefficient and wear when mixed with fluid lubricants. Doping of lanthanide atoms into Na-titanate nanotubes was accomplished via ion exchange reactions. The lanthanide-doped titanate nanotubes exhibited enhanced photoluminescence in the visible and IR optical ranges.[98]

"Chimie douce"

The synthesis of various metal oxide NTs (such as Na$_{2-x}$H$_x$Ti$_2$O$_5$,[99] Ti(HPO$_4$)$_2$,[100] VO$_x$,[101] Ln$_2$O$_3$, Ln(OH)$_3$[102] and others) were reported. Typically, these syntheses involves hydrothermal treatment of the bulk layered compounds at temperatures on the order of 150-230 °C, in the presence or in the absence of organic templates.

The growth mode of titanate nanotubes[99] can be taken as an example to show the general synthetic mechanism of NTs in the absence of a template and at low temperatures (< 200 °C). In the first step, the TiO$_2$ powder was treated under hydrothermal conditions yielding the layered titanate Na$_2$Ti$_2$O$_5$. The solid was then washed at ambient temperature with HCl solutions. The formation of titanate NTs took place during this step in which Na$^+$ ions present in the interlayer space were replaced by H$^+$, causing a shrinkage of the interlayer lattice spacing. This process caused peeling of the titanate layers and subsequent scrolling into NTs.

The synthesis of two-dimensional misfit layered nanotubes (*vide infra*) is not limited to metal chalcogenides, but was also extended to misfit oxide MLC, such as Ca$_3$Co$_4$O$_9$ (denoted for simplicity Ca$_2$CoO$_3$-CoO$_2$ see **Fig. 9a**).[103] The MLC Ca$_3$Co$_4$O$_9$ has attracted significant interest aweing to its potential as promising thermoelectric material. Furthermore, this MLC exhibit excellent thermal and chemical stabilities at elevated temperatures, and reduced toxicity. CaCoO$_3$-CoO$_2$ has a misfit layered structure (**Figure 9a**), consisting of an alternate stacking of edge-sharing octahedral CoO$_2$ layers and distorted rocksalt-type Ca$_2$CoO$_3$ layers along the *c*-axis. Both subsystems are monoclinic, and their lattice parameters coincide along the *a*- and *c*-directions. However, the lattice is incommensurate along the *b*-direction.

The NTs were obtained by means of a hydrothermal treatment of the native bulk MLC in basic suspension at a temperature of 200 °C. The mechanism proposed in this case consists of two steps reaction (see **Fig. 9b**). In the first step the exfoliation of superficial crystalline layers was promoted by the intercalation of Na$^+$ and OH$^-$ ions accompanied by shaving off a CaO layer. Subsequently, scrolling of the sheets occurred due to the tension generated by the loss of inversion symmetry in the lattice, and yielding misfit CaCoO$_2$-CoO$_3$ NTs (see **Fig. 9b**). These NTs present interesting optoelectronic properties. Their optical band gap, which varies between 1.9-2.1 eV, was recently shown to be independent of NTs' geometry.[104] In addition, they possess strongly bound intralayer excitons (up to 0.5 eV binding energy). For these reasons, these NTs could be suitable for optoelectronic applications at the near-infrared to visible (~1.5–2 eV) regions. [104]
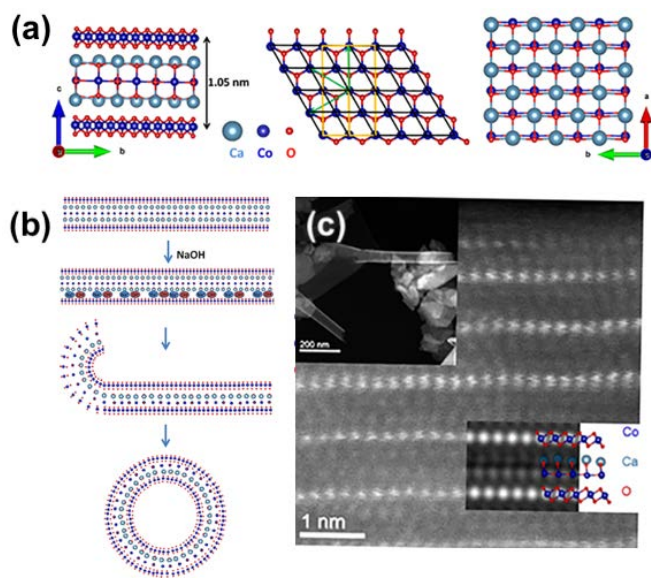
Figure 9. (a) Schematic illustration of the lattice of the bulk Ca_2CoO_3-CoO_2 MLC; (b) Leaching of CaO layer from the bulk MLC through hydrothermal treatment and formation of the nanotube; (c) HAADF-STEM image of the $CaCo_2$-CoO_2 MLC tube. The calculated structure overlaid on the experimentally observed lattice (adapted from Ref. 104 with permission of the ACS).

$Ln(OH)_3$ NTs (Ln= Dy, Ho,[105] Ce,[106] Pr, Sm, Gd, Y, Tb,[107] and Er[108]) have been obtained by hydrothermal synthesis through a dissolution-recrystallization process starting from the corresponding metal oxide (or metal nitrate) in alkaline conditions at 120 °C with yields close to 100%. $Ln(OH)_3$ NTs, that are characterized by a hexagonal quasi-layered structure, which resembles the graphite crystalline layers, can be used as a precursor to obtain Ln_2O_3 or Ln_4O_7 [107] NT compounds in spite of the fact that these materials consist of a tri-dimensional lattice structure. The synthesis of Ln_2O_3, Ln_4O_7 and LnO_2OH nanotubes was accomplished by calcination of $Ln(OH)_3$ NTs in air at temperatures in the range of 450 °C, employing a slow heating rate (1 °C/min).[107]

β-$NaMF_4$ NTs (M=Y, Pr, Sm, Gd, Tb, Dy and Er) were obtained by hydrothermal *in situ* ion-exchange reaction from the corresponding $Ln(OH)_3$ NTs in the presence of HF and NaF at a temperature of 120 °C.[109] The similarity between the crystal structures of the hydroxide and the fluoride compounds and the identical value of the *c*-axis promoted the topotactic substitution of OH$^-$ ions with F$^-$ and the subsequent formation of the most stable hexagonal $NaMF_4$ crystalline layers.

The hydrothermal synthesis of $Ti(HPO_4)_2$,[100] VO_x,[101] GaS and GaSe[102] NTs in the presence of different organic templates have been reported as well. Typically, these syntheses are characterized by the use of a long chain amines that play the role of template and a structure directing agent. The key for accomplishing these syntheses lies in the ability of the aliphatic amines to self-assemble into wire-shaped aggregates due largely to the hydrophobic nature of the aliphatic chains. The hydrophilic amino groups act as a nucleation surface inducing the precipitation of the crystalline layers in tubular structures. Typically, the amines remain confined in between the layers and the diameter of the nanowire is determined by the length of the self-assembled alkyl group moiety. Unfortunately, these materials are unstable as free standing structures, limiting their application to conditions in which the organic templates are not degraded. Incidentally, the GaS nanotubes were tested as active material for lithium ion batteries anodes demonstrating satisfactory results, i.e. 251-317 mA h g^{-1} capacity at 10 mA g^{-1}.[109]

A few recent reports on the synthesis of binary nanotubes with potentially important applications are due. In one study, WS_2 nanotubes were obtained by annealing a sputtered tungsten film in the presence of sulphur vapor at 950 °C.[110]

Boron nitride nanotubes are the subject of intense research for variety of applications, including for thermal management, water filtration, piezoelectric devices etc. Recently, BN nanotubes (BNNT) were synthesized using atomic layer deposition (ALD) of precursors onto electrospun carbon nanofibers and successive high-temperature annealing to remove the carbon fibers and crystallize the BN nanotubes.[111] In another study, WS_2 nanotubes were obtained by annealing a sputtered tungsten film in the presence of sulphur vapor at 950 °C.[112] BNNT with an average radius of 38 nm and about 1 micron in length made of a few walls, were prepared in a scalable fashion by reacting boric acid and ammonia over copper nanoparticles deposited on conductive tungsten substrate.[112] The copper was selected due to the limited solubility of boron and nitrogen in this metal. The tungsten substrate was used due to its chemical inertness and chemical inertness at the relevant temperatures (ca. 1050 °C).

It is worth mentioning that all these works as well as previous ones devoted to the synthesis of BNNTs at low temperature,[80] have not been very successful for high quantity/quality production of BNNTs. In fact, the main advances regarding the synthesis of BNNTs have been obtained via high temperature (higher than 4000K) methods as laser vaporization and plasma torch.[113-116] Arenal et al. reported the production of significant amounts of single-walled NTs and proposed a root-based growth mechanism of these NTs.[113] This growth mechanism is based on the vaporization of different boron compounds (including BN) and the formation of boron droplets which react with nitrogen present in the reaction chamber (either injected or coming from the decomposition of BN). The reaction between these two precursors is at the origin of the BNNTs. This growth mechanism allowed further developments of related synthetic methods, which improved the yield and, at some point, the purity of the produced BN nanostructures.[114-116] In this way, in 2009 and 2014 large-scale production of small-diameter BNNTs has been reported by plasma torch synthesis methods.[115,116] However, even if these works represent a significant improvement in the production of such

nanostructures, the presence of other sub-products (as B-based nanostructures, including h-BN platelets/fragments…) is impeding and limiting the applications of these NTs.

Nanotubes from ternary MLC compounds

The exposure of mixtures of SnS_2 and Bi powder (5:1) in the presence of a minute amount of Sb_2S_3 to a temperature gradient of 780-250 °C led to the production of considerable amounts of $SnS-SnS_2$ NTs and nanoscrolls. In addition, a minor amount of SnS_2 NTs was also obtained.[54] The mechanism behind the formation of these nanostructures involves the vapour-liquid-solid (VLS) catalytic activity of Bi. Due to its relative high vapour pressure the Bi evaporates and reacts with sulphur condensing on the SnS_2 platelet surface. The sulfurization of the Bi/Sb droplets provides the nucleation sites for the formation of the $SnS-SnS_2$ NTs. Indeed, small concentrations of Bi and Sb were found to occur along the tube axis underscoring their catalytic role in the nanotube growth.
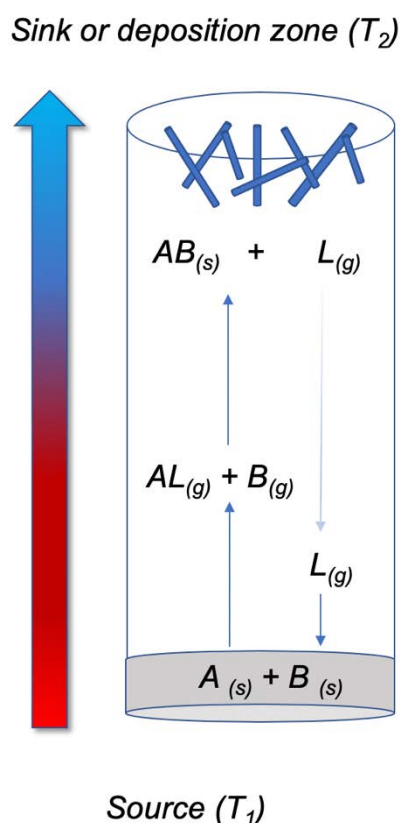

Figure 10. Schematic rendering of the CVT reactions involved in the formation of MLC NTs.

The synthesis of $LnS-CrS_2$ and $LnS-VS_2$ (Ln= rare-earth) misfit NTs was recently reported.[55,117,118] In this case mixtures of $Ln(OH)_3$ and $Cr(OH)_3$ (or $V(OH)_3$)) were converted into misfit sulphides NTs at temperatures on the order of 800 °C under H_2/H_2S flow. At these temperatures a mixed oxide phase was formed which constitute the surface where the growth of misfit sulphide nanotubes takes place by means of the sulfurization, under reducing atmosphere. During the reaction, the oxygen was gradually replaced by the sulphur in a progressive slow diffusion controlled process. The thermal expansion coefficient of the sulphides is generally higher than that of the corresponding oxides. Therefore, the sulfurization process promoted the exfoliation and curling of the nascent crystalline MLC layers. The density of the nanotubes on the substrate surface was shown to depend on the density of grain boundaries available on the oxide substrate. Rapid heating of the substrate promoted fast nucleation of crystallites influencing thereby the surface density of the MLC nanotubes. Incidentally, pristine CrS_2 and VS_2 are not stable as layered compounds. Nevertheless, the charge transfer from the Ln atom, which is more stable in the $Ln^{2+\delta}S$ valence, promotes the stability of the hexagonal layered $Cr^{4-\delta}S_2$ structure in the MLC.

The synthesis of misfit sulphide INTs can also occur in the gas phase, following a chemical vapour transport (CVT) mechanism (see **Fig. 10**). $MS-TaS_2$ (M=Pb, Sn, Sb, Bi[119] and Ln=La, Ce, Pr, Sm, Gd, Ho, Er and Yb [127, 121]) MLC nanotubes have been obtained starting from the metallic sulphides or elemental metal and sulphur in the presence of a catalytic amount of $TaCl_5$, which acted as a catalyst and transport agent. Likewise, $PbS-NbS_2$ NTs have been prepared, starting from a mixture of Nb, PbS and $PbCl_2$.[122] These materials have been obtained via a two-step high-temperature annealing protocol in which the evacuated quartz ampoules were submitted to two opposite temperature gradients. Typically, the preheating of the reactant mixture was performed around 350-400 °C while the growth of the nanotubes occurred at temperatures in the range of 850-900 °C.

In spite of the lack of specific information regarding the intermediates involved in the synthesis of misfit nanotubes, a general growth pattern through chemical vapour transport (CVT) reaction could be delineated. Based on the experimental observations, the presence of a suitable transporting agent in combination with a certain temperature gradient during the growth sequence is essential for the production of the NTs. Mixed metal chlorides are typically formed in small amounts at the high temperature end. The vapors of the two metal chlorides (MCl_x and $TaCl_y$) are transported to the low temperature end of the ampoule, where they react with the sulphur vapor releasing the chlorine atoms allowing the formation of misfit sulphides cluster in the gas phase. These clusters spontaneously bend forming the species that act as a seed for the crystallization of misfit sulphides NTs.

The flexibility of the gas-phase growth mechanism permits incorporating a series of new elements with different sub-lattice units in the tubes, as shown recently in the case of $LaS(Se)-TaS(Se)_2$ NTs.[123] Remarkably, HRSTEM (EELS) analyses showed unequivocally, that the sulphur atoms were bound preferentially to the lanthanum while the selenium atoms were bound to the tantalum. Therefore, a sequence of double La-Ta and S-Se superstructure was obtained in the $LaS-TaSe_2$ nanotubes. In another work, alloyed $LaS-(Nb_xTa_{1-x})S_2$ NTs with varying x were synthesized.[124] Surprisingly, while both bulk compounds are known in the literature[125] and $LaS-TaS_2$

nanotubes are obtained in high yields, the Nb-based analogues were obtained in meagre amounts, only. Indeed, increasing the Nb content in the reaction content (on the expense of Ta), the yield of the nanotubes went down. Not less interesting is the fact that the Nb-rich (Ta-poor) nanotubes were formed in the 1T and not the 2H polytype. However, more work is needed to clarify the Nb and Ta distribution in the hexagonal $(Nb_xTa_{1-x})S_2$ lattice and its influence on the physical properties of such nanotubes, especially at low temperatures. Other MLC nanotubes consisting of ternary and quaternary elements are currently under investigation. One important obstacle for the study of such nanotubes and in particular those containing TaX_2 and NbX_2 (X=S, Se, Te), is their limited stability in the ambient which entails using special handling procedures.

Ternary misfit PbS-SnS$_2$ nanoparticles with fullerene-like structure were obtained by means of solar ablation.[126] Notwithstanding the large (~1.2 nm) interlayer spacing of the MLC structure, the diameter of these hollow-closed nanoparticles was found to be as small as 30 nm. The small diameter of these IF-PbS-SnS$_2$ nanoparticles was attributed to the high temperatures (> 2500 °C) of the reaction, which led to softening of the MLC lattice allowing it to accommodate into IF-NP with very small radii. It has to be emphasized though, that attempts to prepare these nanostructures using conventional ovens and more moderate temperatures (< 1000 °C) were not successful, so far. This fact can be rationalised considering the unique conditions of these experiments, i.e. the high temperatures accompanied by a large temperature gradient ($10^4K/cm^2$), which is crucial for the synthesis of these relatively tiny closed-cage structures.

These studies demonstrate the versatile chemical and physical methods that have been developed for the synthesis of nanotubes and fullerene-like nanostructures from different inorganic layered compounds. Given the rich chemistry and the fact that these 1D nanoparticles were only succinctly studied, there is a large room for a systematic exploration of the physical properties of MLC nanotubes.

Properties

Preface

In order to gain a thorough understanding of the relationship between the structure, chemical composition and the physico-chemical properties of nanotubes, it would be desirable to study a single nanotube at a time using different methodologies. This requirement, however, imposes substantial challenges. For instance, if one wishes to study the structure and chemical composition of a nanotube using high-resolution transmission electron microscope, one has to place the nanotube on a grid. In most cases, the TEM analyses, notorious for the beam damage, should be the last technique among those being used in a series of physical measurements. However, the TEM grid is not a suitable substrate for optical measurements and is not compatible with device fabrication, either. Moreover, analyzing the nanotube in a cryogenic set-up

adds another degree of complexity. This example emphasizes the challenges facing the investigator wishing to analyze an individual nanotube at a time. Albeit the great difficulties, this approach is the most rewarding one in terms of cross-information gained from the use of multitude of techniques and is therefore an important vector in studying the structure-function relationship of nanomaterials in general and nanotubes, in particular.[127-132] Equally important is the fact that, recent advances in *ab-initio* calculations permits quantitative comparison between theory and experimental results of individual nanotubes, which was not there two decades ago.

In virtue of their numerous applications as superior lubricants and for reinforcement of different bulk matrices, the mechanical properties of nanotubes and fullerene-like nanoparticles of WS$_2$ and MoS$_2$, have been investigated in quite a detail for some years, now. Much of these investigations have been reviewed already and will not be further rehearsed here. However, new studies were reported recently and will be briefly described below. Important progress has been recorded in studying the electrical and optical properties of such nanotubes. The optical and electrical properties of nanotubes obtained from misfit layered compounds (MLC) were investigated only succinctly. The catalytic; electrocatalytic and electrochemical behavior of 2D nanomaterials are currently explored to a great deal. Little attention has been paid, relatively speaking, to nanotubes and fullerene-like nanoparticles of other 2D materials, which will be discussed below.

Mechanical and tribological characteristics

Tribological characterization

Extensive efforts have been paid in recent years to study the mechanical and tribological properties of IF/INT of WS$_2$ and MoS$_2$. Few recent works were dedicated to the study of the tribological properties of IF-MoS$_2$ nanoparticles produced by laser ablation in solution;[133] plasma enhanced chemical vapor deposition (PECVD)[134] and microwave assisted synthesis.[135] Using laser ablation in solution resulted in IF nanoparticles with average size of 29 nm. These small nanoparticles could access the contact area of the reciprocating surfaces, preventing thereby the direct contact between the two metal surfaces passing by each other. Furthermore, their ability to roll and gradually exfoliate made these nanoparticles very effective lubricants under very high loads (> 2 GPa). Conversely, MoS$_2$ flakes suffered rapid oxidation under similar conditions.[133] Jacobson and co-workers compared the tribological properties of sputtered WS$_2$ films to electrochemically co-deposited Ni-P films with IF-WS$_2$ nanoparticles.[136] They found that, regardless of the *a-priori* crystalline structure of the two kinds of films, the tribological characteristics under high loads (<1 GPa) were rather similar. They suggested that the main mechanism for the decent tribological behavior of the films was the collapse of their *a-priori* crystalline structure and the alignment of the basal plans of the WS$_2$ nanoslabs in parallel with the coated surface. This alignment afforded facile interlayer shear of the WS$_2$ sheets, and consequently reduced friction and oxidation (wear).

The effect of surface roughness on the lubrication mechanism of MoS_2 nanotubes was systematically investigated on a diamond-like carbon (DLC) coating substrate.[137] It was found that the nanotubes were effective mainly in the boundary lubrication regime, i.e. under high loads where the asperities of the two reciprocating surfaces are in contact with each other. Furthermore, the nanotubes could be retained on the rough surfaces for long periods. Contrarily, sliding of the nanotubes off the contact area was faster on smooth DLC substrate surface. In a recent tribological study, a film made of loosely bound MoS_2 sheets were deposited on a substrate and were tested using a ball-on-flat tribometer[138] under ultra-high vacuum (10^{-3} Pa). The films exhibited an unprecedently low friction coefficient (0.004-0.006). The authors observed nanoscrolls and spherical nanoparticles, which were formed (and gradually destructed) at the interface during the repetitive strokes of the ball-on flat set-up. The small friction coefficient was then attributed to the rolling of the MoS_2 nanospheres and nanoscrolls.

Since lubricating fluids contain various additives it is rather important to find the synergy between the IF/INT nanoparticles with such additives. One main additive is the anti-wear zinc dialkyl dithiophosphate (ZDDP). It was found that the IF/INT nanoparticles provide an effective means for reducing friction in the presence of ZDDP, but the proportion between the concentration of the two additives must be carefully tuned.[139,140] Intriguing results were obtained by mixing MoO_3 nanotubes and zinc dialkyl dithiophosphate (ZDDP), or extreme pressure (EP) alkylated polysulfide olefin with polyalpha olefin 4 (PAO) base oil.[141] Here, MoS_2 crystallites were formed at the reciprocating interface *in-situ* leading to very favorable outcome of the tribological tests. Another progress was accomplished by doping the IF-MoS_2 with minute amounts of rhenium (Re) atoms (<300 ppm). A small fraction (1-2%) of the Re atoms were ionized releasing extra electrons, which diffused to the nanoparticles' surface. The negative surface charge induced by the ionized Re atoms led to self-repelling nanoparticles, which showed little tendency to agglomerate, prompting exceedingly good tribological behavior.[142,143]

Most naturally, tribological characterization cannot be easily experimented with individual nanoparticles. However, the progress with *in-situ* microscopy techniques brings this topic close to realization. The relevance of single nanoparticle experiments to tribological engineering remains, nevertheless questionable. Efforts to emulate tribological experiments with individual IF nanoparticles were recently reported using TEM;[144] scanning electron microscopy[145] and atomic force microscopy.[146] In particular, the sequential rolling, sliding and exfoliation of the nanoparticles was confirmed. The facile shearing of the exfoliated MoS_2 nanosheets provide an additional element to the outstanding tribological performance of the IF nanoparticles. In order to bring these experiments one step closer to tribological engineering conditions, the substrate surface should be functionalized with organic or short polymer molecules which could simulate the effect of IF immersed in lubricating fluids.

New studies shed light on the mechanical stability of nanotubes and fullerene-like nanoparticles under stationary or transient loads. In one such study,[147] synchrotron-based pressure-dependent infrared and Raman spectroscopies of WS_2 nanotubes were carried out using a diamond anvil cell. All the vibrational modes displayed similar hardening trends with ascending pressure except for the Raman-active A_{1g} breathing mode which exhibited almost twice as large Grüneisen parameter, i.e. pressure response. This observation suggested that the nanotube breakdown pathway under strain proceeds through this displacement. This breakdown mechanism was supported by TEM analysis of sonicated and fractured nanotubes. In a related work, the variation of the Raman modes with the number of WS_2 layers was investigated.[148] Here, WS_2 tubes with small diameter (8 nm) were obtained by sulfidization of WO_3 nanowires in an outside-inwards reaction mechanism. Hence, by longer exposure to H_2S at 500 °C the oxide core was gradually converted into tungsten disulfide walls with ever smaller diameter and larger curvature. The inter-layer vibration mode of WS_2 nanotubes- A_{1g} was found to exhibit a redshift of 2.5 cm^{-1} with increasing number of nanotubes layers, which was ascribed to the softening of the mode with increasing curvature strain. This softening overcomes the hardening due to increasing van der Waals interaction in multiwall tubes. Computational study of WS_2 monolayers[149] showed also softening of the Raman active modes under tensile strain (and hardening under compression strain).

Interesting tribological results have also been obtained in BNNTs, opening the way for their use in different applications, as for instance shock-absorbers. Indeed, ultrahigh interlayer friction has been observed in multi-walled BNNTs, when measured *in-situ* in a SEM using a home-made nanomanipulator coupled to a quartz tuning fork.[150] This intershell friction is several orders of magnitude higher than that of CNTs. The authors attribute such differences to the ionic character of these NTs, which is up to 22%. The ionicity of the bonds provokes some faceting between the layers which leads to interlayer locking and a high stiffness.[80] Faceting of multiwall nanotubes with large diameter, most particularly BN nanotubes, is a well-established phenomenon. The faceting leads to stiffening of the nanotubes and larger resistance towards torsion.[151] An astonishing relationship between the tendency for faceting of double wall nanotubes with the same chirality beyond a critical diameter, was observed.[152] Furthermore, the number of facets was determined by the difference in length of the facets of the two (inner and outer) nanotube walls expressed as an integer of the interlayer spacing.

Regarding the mechanical properties of BNNTs, several works have been performed, including reliable *in-situ* TEM measurements in SW- and MWNTs,[153-155] revealing that their elastic modulus varies between 0.8-1.3 TPa, which is close to the one of CNTs. These significant properties make BNNT very good candidates to be part of composite materials. For

instance, BNNTs was shown to reinforce polymer, silica and metallic matrices.[156-159] In the case, of polymeric nanocomposites, BNNTs have shown effective improvement of the elastic modulus (increasing by ~20 %) of polystyrene and polymethyl methacrylate (PMMA) by adding only 1 wt.% of BNNTs. Furthermore, shear strengths of BNNT-epoxy and BNNT-PMMA interfaces of 323 and 219 MPa were reported. In the case of silica matrices, the interfacial strength reaches about 34.7 MPa. All these results indicate that BNNTs are excellent reinforcing nanofiller materials, which can be used for light-weight and high-strength (nano)composites.

Mechanical effects under transient loads have been investigated only scarcely. Probably, the most striking observation was recently reported,[160] whereby a projectile with a speed of some 1000 m/s hit an aluminum foil target filled with IF-WS$_2$ nanoparticles. The authors found that the presence of IF-WS$_2$ in the foil led to a moderation of the impact velocity by over 100 m/s and reduced the transient pressure by at least 2 GPa compared with the reference (Al foil loaded with WS$_2$ platelets). The authors attributed this observation to a "balloon effect", whereby the IF-WS$_2$ composites produced an intriguing inelastic impact, which mitigated the hit by absorbing the shockwave pressures.

In another study the withdrawal of WS$_2$ nanotubes from the surface of a water droplet was investigated.[38] Since these tubes are quite hydrophobic, water molecules are not expected to wet their surface. Indeed the water molecules did not wet the outer surface of the tubes. However, below a critical diameter of the hollow core (ca. 10 nm), strong capillary forces pushed the water molecules into the hollow core of the open-ended nanotubes. The imbibition of water molecules into the narrow core of the nanotubes led to exceedingly high retracting forces with the water surface and necking of the water meniscus, which was confirmed by computer calculations.

Due to the singular properties and characteristics of BNNTs, their application in nanofluidic devices has been explored.[161] BNNTs have been used as nanochannels connecting two different liquid reservoirs. These results suggest that these NTs can be employed as membranes for energy conversion by for example, mixing water different salinities.

Optical and electrical properties

The optical properties of inorganic nanotubes, and in particular those of BN, MoS$_2$ and WS$_2$ have been investigated quite extensively, in both the UV-vis and the IR ranges. Focusing in the transition-metal dichalcogenide nanotubes, given the fact that such multiwall nanotubes are, in general, indirect bandgap semiconductors, the cross-section for luminescence is rather low. Nonetheless, a few recent works demonstrate the unique and rich optical behavior of such nanotubes. In one work,[41] the extinction of WS$_2$ nanotubes with average diameter of 120 nm dispersed in aqueous solutions was studied. The optical extinction revealed a strong scattering component which led to

a red shift and modified lineshape of the spectrum compared to optical absorption measurements. **Fig. 11a** shows the extinction spectrum of the nanotube's suspension (blue curve) and the net absorption of this suspension measured with integrating sphere (black curve).

This behavior was attributed to a strong coupling between the A and B excitons of the WS$_2$ nanotube and axial optical cavity modes along its core, which is represented schematically in **Fig. 11b**.
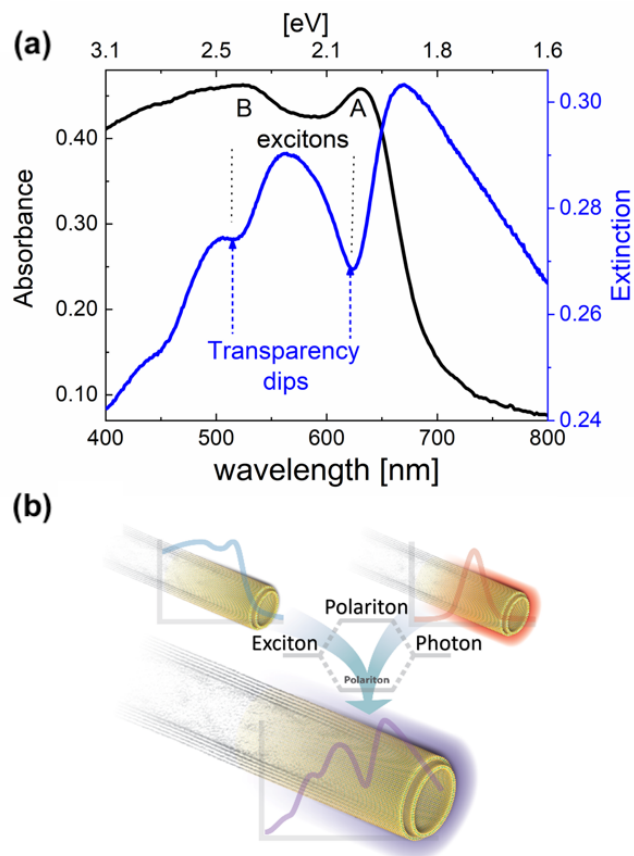

Figure 11. (a) Steady-state absorption (black curve) and extinction (blue curve) spectra of a suspension of WS$_2$ nanotubes with average diameter of 120 nm dispersed in aqueous solution; (b) Schematic illustration of the strong coupling model between cavity mode and the A and B excitons. The strong coupling leads to the dips in the extinction spectra (blue curve) in the wavelengths corresponding to the excitons and the strong light scattering of the nanotubes (adopted from Ref. 41 with permission of the RSC).

Notwithstanding its indirect gap, strong electroluminescence was emitted from a *p-n* junction established by ionic liquids on a single WS$_2$ nanotube.[162] **Fig. 12a** shows a schematic drawing of the electroluminescing device based on single WS$_2$ nanotube and ionic gating, while **Fig. 12b** shows an optical image of the device and its spectral distribution. The electroluminescence spectrum is composed of a strong peak in 1.85 eV associated with the direct transition and a weaker one at 1.4 eV assigned to the indirect transition. In another recent work, polarized

micro-photoluminescnece (micro-PL) of multiwall MoS_2 nanotubes was recently studied.[163,164] Periodic peaks in the micro-PL spectra polarized in the axial direction were observed and attributed to quantized gallery whispering modes which are in resonance with the nanotube core.
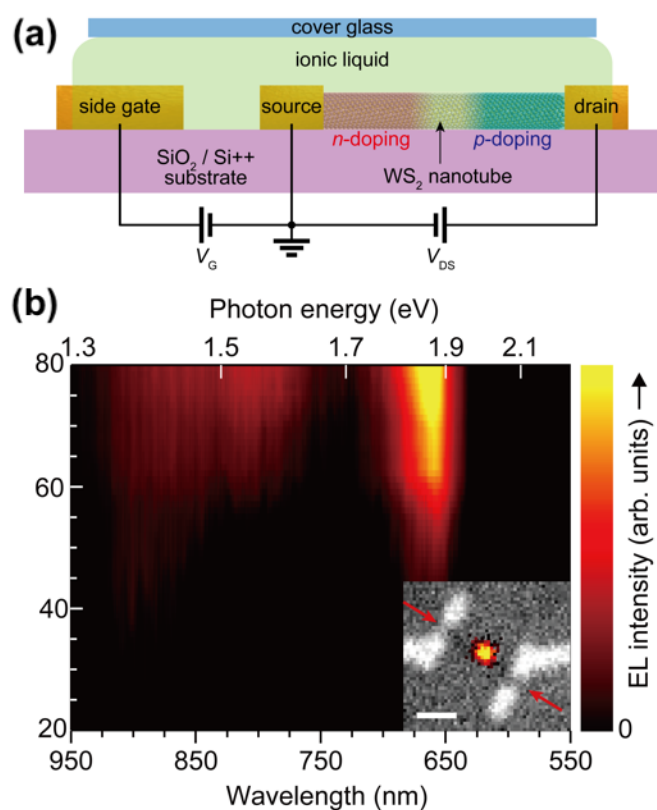

Figure 12. (a) Illustration of a WS_2 nanotube-based field effect transistor (FET) with an ionic liquid gate for optoelectronic experiments; (b) Light emitting diode (LED) operation of a WS_2-based *p-n* junction. Map of the electroluminescence intensity versus the emitted wavelength. The inset shows the image of the EL device with a spatial mapping of the emitted light intensity. White areas correspond to the contacts. The red arrows mark the orientation of the WS_2 nanotube (adopted from Ref. 162 with permission of the IoP).

Recently, new core-shell nanostructures consisting of a gold nanoparticle sheathed with one or a few (fullerene-like) layers of MoS_2 were described.[165,166] Not unexpectedly, these Au@MoS_2 core-shell heterostructures exhibit strong coupling between the excitonic transitions of the MoS_2 shell and the plasmon of the underlying Au nanoparticle core. This coupling led to a strong modulation of the optical spectra in the visible and enhanced Raman scattering and PL emission of these heterostructures. These enhancements were attributed to the surface plasmon-induced electric field, which according to the simulations is localized mainly within the MoS_2 shell.

With the advent of nanofabrication technology electrical devices based on single nanotube, like field effect transistors (FET); electromechanical devices, etc., became more common.

Numerous technological issues related to the fabrication of contacts, selective etching for undercutting and suspending the tubes had to be solved prior to the demonstration of any viable device technology. Recent advances include FET transistors with high on/off ratio;[167,168] electromechanical resonators,[169] etc. Low temperature superconductivity with clear quasi-1D superconductivity characteristics was demonstrated for ionic liquid gated WS_2 nanotubes.[39] Little-Parks oscillations of the supercurrent as a function of the magnetic field, which was applied along the tube axis, was clearly observed. The second harmonic component of the AC supercurrent showed nonreciprocal behavior, which reflected the breaking of inversion symmetry due to the chirality of the nanotube. This study clearly demonstrated that the supercurrent flows in a spiral trajectory on the perimeter of the nanotube. More recently, the quasi-1D characteristics of the supercurrent was validated by showing that the critical temperature-*Tc* decreases with reducing diameter of the nanotubes.[170]

BNNTs possess an isolating character showing a large band gap (close to 6 eV) independently of their number of layers, diameter and chirality.[80, 83, 171] Their optical properties are governed by strong excitonic effects.[172-175] Furthermore, MWBNNTs present also other interesting luminescence characteristics showing some features which correspond to intrinsic structural defects attributed to their faceting.[174] In addition, it has been also reported that one-dimensional guided surface phonon polaritons (SPhPs) can be generated in these NTs. The effective refractive index of SPhPs in BNNTs is very high and it is inversely proportional to the nanotube diameter, allowing their optical tunability.[176,177] This offer opportunities for trapping light at mid-infrared frequencies with the possibility of having a tunable deep-subwavelength light-trapping system in these frequencies. This opens the avenue for potential applications as nano-sensors, nonlinear optics, etc.

Conclusions and Applications - Future Prospects

In summary, this review highlights the recent advances of inorganic nanotubes putting them in context of their 2D (planar) counterparts. Their very interesting properties make them promising materials for use in different technological areas, including catalysis, photovoltaics, energy harvesting, optoelectronic, and others. However, despite this high interest, apart the tribological applications of some of these nanostructures, the development of the wide opportunities offered by such nanomaterials is rather limited. These limitations can be mainly attributed to the difficulties associated with the mass-production of good quality nanotubes. In addition, other aspects concerning, in some of the cases, the complex structure of these inorganic nanotubes also hinders their applications. Indeed, for some of these nanomaterials, their atomic structure, which controls most of their properties, is not fully solved. This is a critical aspect not only for elucidating their properties, but also for getting a better insight on their growth mechanism, which could eventually lead to a progress in their large-scale production.

As a final remark and future prospects, we will also present the most promising applications of some of these inorganic nanotubular structures.

As soon as C_{60} became available in substantial amounts, it was conceived as being an ideal nanoball-bearing[177] which idea has not been materialized. Noting the long history of MoS_2 as solid lubricant,[178] the idea to use IF-WS_2 for this purpose was not far-fetched. However, it remained "on paper" only unless gram quantities of pure IF-WS_2 could be synthesized. Once this step could be accomplished,[179,180] the favorable effect IF-WS_2 nanoparticles as additive to tribological fluids could be confirmed.[44] Unavoidably, however, this idea faced various obstacles before it could be translated into a viable technology. The first challenge was the scaling-up of the production of these nanoparticles via a high-temperature reaction to a large-scale manufacturing process. This process took well over a decade to mature. Furthermore, modern lubricants contain various additives contributing, each, to its long shelf-life, stable operation, oxidation resistance, while others are intended to minimize friction and wear. In order for the IF-WS_2 nanoparticles to work in harmony with the other components of lubricating fluids, a new formulation had to be worked-out, which took many additional years for development. Issues of toxicity and biocompatibility are of major concern and have been also partially addressed. Another technological challenge is the processing of used lubricants at the end of their life-cycle. Presently many of these issues have been resolved and consequently the market-share of this technology (sometime dubbed "NanoLub") is progressing steadily. In the meantime, new applications have been conceived and gradually materialized for the IF-WS_2, including as additive to metal-working fluids, special formulations for high performance bearings, tribological coatings, lubricants for transmission systems, etc.

Polymer composites formulated with nanoparticles are investigated for many years and found numerous applications already, e.g. in aviation. While initial efforts concentrated primarily on naturally occurring fillers, like clays and silicates, more recently efforts have been geared towards using carbon nanotubes and subsequently graphene as fillers to polymer nanocomposites. Fullerene-like nanoparticles and nanotubes of WS_2 suffer from several shortcomings, relative to their carbon analogues. They are larger, heavier and are not as strong. Furthermore, their electrical and thermal conductance are inferior to their carbon analogues. Despite this, they possess several characteristics valuable for the reinforcement of different nanocomposites. In the absence of aromaticity, IF/INT of WS_2 do not show tendency to agglomerate as strongly as their carbon analogues and hence can be dispersed in different matrices more uniformly and without exerting excessive energy. Moreover, due to their being good lubricants, the addition of IF/INT to polymer blends does not lead to large increase in the viscosity, or sometime incur reduced viscosity, which has substantial implications for the processing and production costs of the polymer nanocomposites in industrial

environment. Nanoparticles of MX_2 materials, including IF/INT were found to be relatively nontoxic and benign up to high concentrations (>0.1 mg/ml),[181-183] offering them potential applications in different medical technologies. Another important area of research is in shock absorbance, which is relevant to many applications including the automotive industry, sport, prostheses, self-protecting jackets and many more. Few recent examples to studies in this direction in recent years showed that the addition of IF-WS_2 and even more so-INT-WS_2 can reduce the absorbed shock as much as 50% in metal and polymer matrices.[159,184,185]

Conflicts of interest

In accordance with our policy on <u>Conflicts of interest</u> please ensure that a conflicts of interest statement is included in your manuscript here. Please note that this statement is required for all submitted manuscripts. If no conflicts exist, please state that "There are no conflicts to declare".

Acknowledgements

References

1   G. Aminoff, *Z. Kryst. Minerlog.*, 1921, **56**, 127.
2   2 R. M. Bozorth, *J. Am. Chem. Soc.*, 1922, **44**, 2232.
3   R. G. Dickinson and L. Pauling, *J. Am. Chem. Soc.*, 1923, **45**, 1466.
4   B. Warren and W. L. Bragg, *Z. Kristallogr. - Cryst. Mater.*, 1931, **76**, 201.
5   L. Pauling, *Proc. US Natl. Acad. Sci. U. S. A.*, 1930, **16**, 578.
6   J. Turkevich and J. Hillier, *J. Anal. Chem.*, 1949, **21**, 475.
7   A. T. Waterman, *Phys. Rev.,* 1923, **21**, 540.
8   I. Oftedal, *Norsk Geol. Tidsskr.*, 1927, **9**, 225.
9   J. A. Wilson and A. D. Yoffe, *Adv. Phys.*, 1969, **18**, 193.
10 a. D. Riedel *Crystallography and Crystal Chemistry of Materials with Layered Structures*, F. Levy Ed., Dordecht-Holland-Boston- USA, 1976. b. *Kazuko Motizuki, Series Physics and Chemistry of Layered Compounds Vol.2*, E. Mooser, 1986.
11 a. H. Tributsch, *Ber. Der Bunsenges. Phys. Chem.*, 1977, **81**, 361; b. H. Tributsch, *J. Electrochem. Soc.*,1978, **125**, 1086.
12 G. Kline, K. Kam, D. Canfield and B. A. Parkinson, *Solar Energy Mater.*, 1981, **4**, 301.
13 R. Tenne and A. Wold, *Appl. Phys. Lett.*, 1985, **47**, 707.
14 J. A. Wilson, F. J. Disalvo and S. Mahajan, *Adv. Phys.*, 1975, **24**, 117.

15 W. Rüdorff and H. H. Sick, *Angew. Chern.*, 1959, **71**, 127.

16 F. R. Gamble, F. J. DiSalvo, R. A. Klemm and T. H. Geballe, *Science*, 1970, **168**, 568.

17 R.B. Somoano and A. Rambaum, *Phys. Rev. Lett.*, 1972, **27**,402.

18 M. S. Whittingham and F. D. Gamble, Jr., *Mater. Res. Bull.*, 1975, **10**, 363.

19 K. Mizushima, P. C. Jones, P. J. Wiseman and J. B. Goodenough, *Solid State Ionics*, 1981, **3-4**, 171.

20 S. C. Schuman and H. Shalit, *Catal. Rev.* 1971, **4**, 245.

21 C. J. H. Jacobsen, E. Törnqvist and H. Topsøe, *Catal. Lett.,* 1999, **63**, 179.

22 P. Joeansen, R. F. Frindt and S. R. Morrison, *Mater. Res. Bull.*, 1986, **21**, 457.

23 A. Koma, K. Sunouchi and T. Miyajima*, J. Vac. Sci. Tech. B*, 1985, **3**, 724.

24 K. S. Novoselov, A. K. Geim, S. V. Morozov, D. Jiang, M. I. Katsnelson, I. V. Grigorieva, S. V. Dubonos and A. A. Firsov, *Nature*, 2005, **438**, 197.

25 B. Radisavljevic, A. Radenovic, J. Brivio, V. Giacometti and A. Kis, *Nature Nanotech.*, 2011, **6**, 147.

26 K. F. Mak, C. Lee, J. Hone, J. Shan and T. F. Heinz, *Phys. Rev. Lett.*, 2010, **105**, 136805.

27 X. Cui, G.-H. Lee, Y. D. Kim, G. Arefe, P.Y. Huang, C.-H. Lee, D.A. Chenet, X. Zhang, L. Wang, F. Ye, F. Pizzocchero, B.S. Jessen, K. Watanabe, T. Taniguchi, D. A. Muller, T. Low, P. Kim and J. Hone, *Nature Nanotech.*, 2015, **10**, 534.

28 T. F. Bates, L. B. Sand and J. F. Mink, *Science*, 1950, **111**, 512.

29 E. J. W. Whittaker, *Acta Cryst.*, 1955, **8**, 571.

30 H. W. Kroto, J. R. Heath, S. C. O'Brien, R. F. Curl and R. E. Smalley, *Nature*, 1985, **318**, 162.

31 S. Iijima, *Nature*, 1991, **354**, 56.

32 R. Tenne, L. Margulis, M. Genut and G. Hodes, *Nature*, 1992, **360**, 444.

33 L. Margulis, G. Salitra, R. Tenne and M. Talianker, *Nature,* 1993, **365**, 113.

34 Y. Feldman, E. Wasserman, D. J. Srolovitz and R. Tenne, *Science*, 1995, **267**, 222.

35 R.A. Evarestov, *Theoretical Modeling of Inorganic Nanostructures*, Springer, Heidelberg, 2015.

36 I. Kaplan-Ashiri, S.R. Cohen, K. Gartsman, V. Ivanovskaya, T. Heine, G. Seifert, I. Wiesel, H.D. Wagner and R. Tenne, *Proc. US Natl. Acad. Sci. US,* 2006, **103**, 523.

37 I. Lahouij, F. Dassenoy, L. de Knoop, J.-M. Martin and B. Vacher, *Tribol. Lett.*, 2011, **42**, 133.

38 O. Goldbart, S.R. Cohen, I. Kaplan-Ashiri, P. Glazyrina, H.D. Wagner, A. Enyashin and R. Tenne, *Proc. US Natl. Acad. Sci.*, 2016, **113**, 13624.

39 F. Qin, W. Shi, T. Ideue, M. Yoshida, A. Zak, R. Tenne, T. Kikitsu, D. Inoue, D. Hashizume, and Y. Iwasa, *Nature Comm.*, 2017, **8**, 14465.

40 N. Zibouche, P. Philipsen, and A. Kuc, *J. Phys. Chem. C,* 2019, **123**, 3892.

41 L. Yadgarov, B. Visic, T. Abir, R. Tenne, A. Polyakov, R. Levi, T.V. Dolgova, V.V. Zubyuk, A.A. Fedyanin, E.A. Goodilin, T. Ellenbogen, R. Tenne and D. Oron, *Phys.Chem.Chem.Phys.*, 2018, **20**, 20812.

42 D. R. Kazanov, A. V. Poshakinskiy, V. Yu. Davydov, A. N. Smirnov, I. A. Eliseyev, D. A. Kirilenko, M. Remskar, S. Fathipour, A. Mintairov, A. Seabaugh, B. Gil and T. V. Shubina, *Appl. Phys. Lett.* 2018, **113**, 101106.

43 A. N. Enyashin, S. Gemming and G. Seifert, Springer Series in Mater. Sci., 2006, **93**, 33.

44 L. Rapoport, Yu. Bilik, Y. Feldman, M. Homyonfer, S.R. Cohen, and R. Tenne, *Nature*, 1997, **387**, 791.

45 M. Chhawolla and G.A.J. Amaratunga, *Nature*, 2000, **407**, 164.

46 M. Pardo, T. Shuster-Meiseles, S. Levin-Zaidman, A. Rudich, Y. Rudich, *Environ. Sci. Technol.,* **2014**, *48*, 3457.

47 W. Sterzel, *Naturwissenschaften,* 1966, **53**, 199.

48 L. Schmidt, *Phys. Lett. A* 1970, **31**, 551.

49 E. Makovicky and B. Hyde, *Inor. Chem.*, 1981, **48**, 101.

50 a. G. Wiegers and A. Meerschaut, *Mater. Sci. Forum*, 1992, **100-101**, 101; b. G. A. Wiegers and A. J. Meerschaut, *J. Alloys Compd.*, 1992, **178,** 351.

51 L. Guemas, P. Rabu, A. Meerschaut, J. Rouxel, *Mater. Res. Bull.*, 1988, **23**, 1061.

52 S.Y. Hong, R. Popovitz-Biro, Y. Prior and R. Tenne, *J. Am. Chem. Soc.*, 2003, **125**, 10470.

53 Y. Ohno**,** *J. Solid State Chem.*, 2005, **178**, 1539.

54 G. Radovsky, R. Popovitz-Biro, M. Staiger, K. Gartsman, C. Thomsen, T. Lorenz, G. Seifert and R. Tenne, *Angew. Chem. Int. Ed.*, 2011, **123**, 12524.

55 L.S. Panchakarla, R. Popovitz-Biro, L. Houben, R.E. Dunin-Borkowski and R. Tenne, *Angew. Chem. Int. Ed.*, 2014, **126**, 7040.

56 B. Visic, L.S. Panchakarla and R. Tenne, *J. Am. Chem. Soc.*, 2017, 139, 12865.

57 T.F. Bates, F.A. Hildebrand and A Swineford, *Am. Miner.*, 1950, **35**, 463.

58 T.F. Bates, *Am. Miner.*, **44**, 1959, 78.

59 P.D.G. Cradwick, V.C. Farmer, J.D. Russell, C.R. Masson, K. Wada, and N. Yoshinaga, *Nature*, 1972, **240**, 187.

60 I. Bottero, B. Bonelli, S. E. Ashbrook, P. A. Wright, W. Zhou, M.Tagliabue, M. Armandia and E. Garronea, *Phys. Chem. Chem. Phys.,*,2011**13**, 744.

61 M. Ookawa, Y. Inoue, M. Watanabe, M. Suzuki and T.Yamaguchi, *Clay Science*, 2006 , **12**, 280.

62 E. Shafia, Synthesis and Characterization of Fe-modified Imogolite Nanotubes, Politecnico di Torino, 2015.

63 A. Avellan, C. Levard, N. Kumar, J. Rose, L. Olivi, A. Thill, P. Chaurand, D. Borschneck and A. Masion, *RSC Advances*, 2014, **4**, 49827.

64 P. Yuan, D. Tan and F. Annabi-Bergaya, *Applied Clay Science*, 2015, **112–113**, 75.

65 A. Kuc and T. Heine, *Adv. Mat.,* 2009*,* **21**, 4353.

66 G. Monet, M.S. Amara, S. Rouzière, E. Paineau, Z. Chai, J.D. Elliott, E. Poli, L.-M. Liu, G. Teobaldi and P. Launois, *Nat. Commun.*, **2018**, 9, 2033.

67 E. Paineau, *Appl. Sci.*, 2018, **8**, 1921.

68 R. Kreizman, S.-Y. Hong, J. Sloan, R. Popovitz-Biro, A. Albu-Yaron, G. Tobias, B. Ballesteros, B.G. Davis, M.L.H. Green and R. Tenne, *Angew. Chem. Int. Ed.*, 2009, **48**, 1230.

69 R. Kreizman, A. N. Enyashin, F. L. Deepak, A. Albu-Yaron, R. Popovitz-Biro, G. Seifert and R. Tenne, *Adv. Funct. Mater.*, 2010, **20**, 2459.

70 L. Cabana, B. Ballesteros, E. Batista, C. Magén, R. Arenal, J. Oró-Solé, R. Rurali, and G. Tobias, *Advanced Materials,* 2014, **26**, 2016.

71 S. Sandoval, E. Pach, B. Ballesteros and G. Tobias, *Carbon*, 2017, **123**, 129.

72 S. Sandoval, D. Kepić, Á. -P. del Pino, E. György, A. Gómez, M. Pfannmoeller, G. Van Tendeloo, B. Ballesteros and G. Tobias, *ACS Nano,* 2018, **12**, 6648.

73 N. M. Batra, A. E. Ashokkumar, J. Smajic, A. N. Enyashin, F. L. Deepak and P. M. F. J. Costa, *J. Phys. Chem. C*, 2018, **122**, 24967.

74 X. C. Song, Y. F. Zheng, Y. Zhao and H. Y. Yin, *Mater. Lett.*, 2006, **60**, 2346

75 Y. Wang, Z. Ma, Y. Chen, M. Zou, M. Yousaf, Y. Yang, L. Yang, A. Cao and R. P. S. Han, *Adv. Mater.*, 2016, **28**, 10175.

76 J. Wang, J. Liu, H. Yang, Z. Chen, J. Lin and Z. X. Shen, *J. Mater. Chem. A*, 2016, **4**,7565.

77 B. Shen, H. Xie, L. Gu, X. Chen, Y. Bai, Z. Zhu and F. Wei, *Adv. Mater.,*2018, **2**, 1803368.

78 B. Jin, X. Zhou, L. Huang, M. Lick(lederer, M. Yang and P. Schmuki, *Angew. Chem. Int. Ed*., 2016, **128**, 12440.

79 R. Nakanishi, R. Kitaura, J.H. Warner, Y. Yamamoto, S. Arai, Y. Miyata, and H. Shinohara, *Sci. Rep*., 2013, **3**, 1385.

80 R. Arenal, X. Blase, A. Loiseau, *Adv. Phys*., 2010, **59**, 101.

81 Mickelson, W.; Aloni, S.; Han, W.-Q.; Cumings, J.; Zettl., *Science,* 2003, **300**, 467.

82 D. Golberg, Y. Bando, K. Fushimi, M. Mitome, L. Bourgeois, and C.C. Tang, *J. Phys. Chem. B*, 2003, **107**, 8726.

83 R. Arenal, A. Lopez-Bezanilla, *ACS Nano*, 2014, **8**, 8419.

84 X. Zhou, F.-C. Hsia, Y. Xue, D.-M. Tang, O. Cretu, C. Zhang, M. Mitome, Y. Bando, T. Sasaki, D. Golberg. *Phys. Status Solidi – Rap. Res. Let.*, 2018, **6**, 1800576.

85 T. Pham, A. Fathalizadeh, B. Shevitski, S. Turner, S. Aloni and A. Zettl. *Nano Let.*, 2016, **16**, 320.

86 K.E. Walker, G.A., Rance, Á. Pekker, H.M. Tóháti, M.W. Fay, R.W. Lodge, C.T. Stoppiello, K. Kamarás, A.N. Khlobystov, *Small Meth.*, 2017, **1**, 1700184.

87 T. Xu, Y. Zhou, X. Tan, K. Yin, L. He, F. Banhart and L. Sun, *Adv. Funct. Mater.*, 2017, **27**, 1603897.

88 A. Yella, E. Mugnaioli, M. Panthöfer, H. A. Therese, U. Kolb and W. Tremel, *Angew. Chem. Int. Ed.*, 2009, **48**, 6426.

89 O. Brontvein, D. G. Stroppa, A. Albu-Yaron, M. Levy, D. Feuerman, L. Houben, R. Tenne and J. M. Gordon, *J. Am. Chem. Soc.* 2012, **134**, 16379.

90 M. Weng, M. Zhang, T. Yanase, F. Uehara, T. Nagahama and T. Shimada, *Jpn. J. Appl. Phys.*, 2018, **57**, 30304.

91 O. Brontvein, L. Houben, R. Popovitz-Biro, M. Levy, D. Feuermann, R. Tenne and J.M. Gordon, *Nano*, 2017, **12**, 1750030.

92 P. Ayala, R. Arenal, A. Loiseau, A. Rubio and T. Pichler, *Rev. Mod. Phys.*, 2010, **82**, 1843.

93 P. Ayala, R. Arenal, M. Rummeli, A. Rubio, T. Pichler, *Carbon* 2010, **48**, 575.

94 R. Arenal, K. March, C.P. Ewels, X. Rocquefelte, M. Kociak, A. Loiseau and O. Stéphan, *Nano Lett.,* 2014, **14**, 5509.

95 L. Francis, A. Mayoral and R. Arenal, *Advanced Transmission Electron Microscopy: Applications to Nanomaterials*, Eds. Springer, 2015.

96 L. Yadgarov, R. Rosentsveig, G. Leitus, A. Albu-Yaron, A. Moshkovith, V. Perfilyev, R. Vasic, A. I. Frenkel, A.N. Enyashin, G. Seifert, L. Rapoport and R. Tenne, *Angew. Chem. Int. Ed.*, 2012, **51**, 1148.

97 R. Rosentsveig, L. Yadgarov, Y. Feldman, S. Shilstein, R. Popovitz-Biro, B. Visic, A. Sedova, S. R. Cohen, Y. Li, A.I. Frenkel and R. Tenne, *Particle and Particle Systems Charact*., 2018, **35**, 1700165.

98 T. M. F. Marques, C. Luz-Lima, M. Sacilloti, K. Fujisawa, N. Perea-Lopez, M. Terrones, E. N. Silva, O. P. Ferreira and B. C. Viana, *J. Nanomater.,* 2017, **2**, 3809807.

99 C.-C. Tsai and H. Teng, *Chem. Mater*, 2006, **18**, 367.

100 Z. Yin, Y. Sakamoto, J. Yu, S. Sun, O. Terasaki and R. Xu, *J. Am. Chem. Soc.*, 2004, **126**, 8882.

101 M. Niederberger, H.-J. Muhr, F. Krumeich, F. Bieri, D. Gunther and R. Nesper, *Chem. Mater.*, 2000, **12 (7)**, 1995.

102 L. Tao, C.G. Sun, M.-L. Fan, Q. Liu, C.-J.Huang, H.-S. Zhai, H.-L.Wu and Z.-S. Chao, *Studies in Surface Science and Catalysis*, 2007,**165**,339.

103 L. S. Panchakarla, L. Lajaunie, A. Ramasubramaniam, R. Arenal and R. Tenne, *ACS Nano*, 2016, **10 (60)**, 6248.

104 L. Lajaunie, A. Ramasubramaniam, L.S. Panchakarla, and R. Arenal, *Appl. Phys. Lett*., 2018, **113**, 031102.

105 A.-W. Xu, Y.-P. Fang, L.-P. You and H.-Q. Liu, *J. Am. Chem. Soc.*, 2003, **125**, 1494.

106 W.-Q. Han, L. Wu and Y. Zhu, *J. Am. Chem. Soc.*, 2005, **127** (37), 12814.

107 Y.-P. Fang, A.-W. Xu, L.-P. You, R.-Q. Song, J.C. Yu, H.-X. Zhang, Q. Li and H.-Q. Liu, *Adv. Funct. Mater.,* 2003*,* **13**, *995.*

108 F. Zhang and D. Zhao, *ACS Nano*, 2009, **1**, 159.

109 A. Seral-Ascaso, S. Metel, A. Pokle, C. Backes, C. J. Zhang, H. C. Nerl, K. Rode, N. C. Berner, C. Downing, N. McEvoy, E. Muñoz, A. Harvey, Z. Gholamvand, G. S. Duesberg, J. N. Coleman and V. Nicolosi, *Nanoscale*, 2016, **8**, 11698.

110 E. Hossain, A. Azizur Rahman, R.D. Bapat, J.B. Parmar, A.P. Shah, A. Arora, R. Bratschitsch and A. Bhattachary, *Nanoscale* 2018, **10**, 16683.

111 a. W. Hao, C. Marichy and A. Brioude, *Environ. Sci.: Nano*, 2017, **4**, 2311; b. M. Weber, I. Iatsunskyi, E. Coy, P. Miele, D. Cornu and M. Bechelany, *Adv. Mater. Interfaces,* 2018, **5**, 1800056.

112 V. Kumar, P. C. Maity, D. Lahiri and I. Lahiri, *CrystEngComm*. 2018, **20**, 2713.

113 R. Arenal, O. Stephan, J.-L. Cochon, and A. Loiseau, *J. Am. Chem. Soc.,* 2007, **129**, 16183.

114 M.W. Smith, K.C. Jordan, C. Park, J.-W. Kim, P.T. Lillehei, R. Crooks, J.S. Harrison, *Nanotechnology,* 2009, **20**, 505604.

115 K.S. Kim, C.T. Kingston, A. Hrdina, M.B. Jakubinek, J. Guan, M. Plunkett and B. Simard, *ACS Nano*, 2014, **8**, 6211.

116 A. Fathalizadeh, T. Pham, W. Mickelson and A. Zettl, *Nano Lett.* 2014, **14**, 4881.

117 L. S. Panchakarla, G. Radovsky, L. Houben, R. Popovitz-Biro, R. E. Dunin-Borkowski and R. Tenne, *J. Phys. Chem. Lett.,* 2014, **5**, 3724.

118 L.S. Panchakarla, L. Laujaunie, R. Tenne and R. Arenal, *J. Chem. Phys. C*, 2016, **120**, 15600.

119 G. Radovsky, R. Popovitz-Biro and R. Tenne, *Chem. Mater.*, 2014, **26**, 3757.

120 G. Radovsky, R. Popovitz-Biro, T. Lorenz, J.-O. Joswig, G. Seifert, L. Houben, R. E. Dunin-Borkowski and R. Tenne, *J. Mater. Chem. C.*, 2016, **4**, 89.

121 M. Serra, D. Stolovas, L. Houben, R. Popovitz-Biro, I. Pinkas, F. Kampmann, J. Maultzsch, E. Joselevich and R. Tenne, *Chem. Eur. J.*, 2018, **24**, 1.

122 G. Radovsky, R. Popovitz-Biro, D. G. Stroppa, L. Houben and R. Tenne, *Acc. Chem. Res.*, 2014, **2**, 406.

123 L. Lajaunie, G. Radovsky, R. Tenne and R. Arenal, *Inorg. Chem.*, 2018, **57** (2), 747.

124 D. Stolovas, M. Serra, R. Popovitz-Biro, I. Pinkas, L. Houben, J.J. Calvino, E. Joselevich, R. Tenne, R. Arenal and L. Lajaunie, *Chem. Mater., 2018, **30** (24), 8829.*

125 G. Wiegers, A. Meetsma, S. Van Smaalen, R. Haange, J. Wulff, T. Zeinstra, J. De Boer, S. Kuypers, G. Van Tendeloo, J. Van Landuyt, S. Amelinckx, A. Meersehaut, P. Rabu and J. Rouxel, *Solid State Comm*., 1989, **70**, 409.

126 O. Brontvein, A. Albu-Yaron, M. Levy, D. Feuerman, R. Popovitz-Biro, R. Tenne, A. Enyashin and J. M. Gordon., *ACS Nano*, 2015, **8**, 7831.

127 M.Y. Sfeir, T. Beetz, F. Wang, L. Huang, X.M.H. Huang, M. Huang, J. Hone, S.O. Brien, J.A. Misewich, T.F. Heinz, L. Wu, Y. Zhu, L.E. Brus, S. O'Brien, J.A. Misewich, T.F. Heinz, L. Wu, Y. Zhu and L.E. Brus, *Science*, 2006, **312**, 554.

128 D. Levshov, T. Than, R. Arenal, V. N. Popov, R. Parret, M. Paillet, V. Jourdain, A. A. Zahab, T. Michel and J.-L. Sauvajol, *Nano Letters*, 2011, **11**, 4800.

129 K. Liu, J. Deslippe, F. Xiao, R.B. Capaz, X. Hong, S. Aloni, A. Zettl, W. Wang, X. Bai, S.G. Louie, E. Wang and F. Wang, *Nat. Nanotechnol.*, 2012*,* **7**, 325.

130 R. Arenal, P. Löthman, M. Picher, T. Than, M. Paillet and V. Jourdain, *J. Phys. Chem. C.*, 2012, **116**, 14103.

131 D.I. Levshov, R. Parret, H.-N. Tran, T. Michel, T. Thanh Cao, V.C. Nguyen, R. Arenal, V.N. Popov, S.B. Rochal, J.-L. Sauvajol, A.-A. Zahab and M. Paillet, *Phys. Rev. B*, 2017, **96**, 195410.

132 D.I. Levshov, H.N. Tran, M. Paillet, R. Arenal, X.T. Than, A.A. Zahab, Y.I. Yuzyuk, J.-L. Sauvajol and T. Michel, *Carbon*, 2017, **114**, 141.

133 T. Luo, X. Chen, L. Wang, P. Wang, C. Li, H. Zeng, B. Cao, *Tribol. Int.,* 2018, 122, 119.

134 S.E. Alexandrov, K.S. Tyurikov, D.A. Kirilenko, A.V. Redkov, and A.A. Lipovskii, *Adv. Mater. Inter.*, 2017, **4**, 1700241.

135 Z. Liu, L. Zhang, R. Wang, S. Poyraz, J. Cook, M.J. Bozack, S. Das, X. Zhang, L. Hu, *Sci Rep.*, 2016, **6**, 22503.

136 F. Gustavsson, F. Svahn, U. Bexell, S. Jacobson, *Surface & Coatings Tech.,* 2013, **232**, 616.

137 J. Kogovšek, M. Remškar, M. Kalin, *Wear*, 2013, **303**, 361.

138 K. Hou, M. Han, X. Liu, J. Wang, Y. He and S. Yang, *Nanoscale*, 2018, **10**, 19979.

139 M. Rodrıguez Ripoll, A. Naveira Suarez, M. Remskar, R. Rosentsveig, *Tribol. Lett.*, 2015, **59**, 26.

140 P.U. Aldana, F. Dassenoy, B. Vacher, T. LeMogne, B. Thiebaut, *Tribol. Int.*, 2016, **102**, 213.

141 M.R. Ripoll, A. Tomala, C. Gabler, G. Dražić, L. Pirkerd and M. Remškar, *Nanoscale,* 2018, **10**, 3281.

142 L. Yadgarov, V. Petrone, R. Rosentsveig, Y. Feldman, R. Tenne and A. Senatore, *Wear*, 2013, **297**, 1103.

143 A. Sedova, R. Ron, O. Goldbart, O. Elianov, L. Yadgarov, N. Kampf, R. Rosentsveig, D. Shumalinsky, L. Lobik, B. Shay, J. Moshonov, H.D. Wagner and R. Tenne, *Nanomater. & Energy,* 2014*, 4*, 30.

144 I. Lahouij, F. Dassenoy, B. Vacher, and J.-M. Martin, *Tribol. Lett.*, 2011, **45**, 131.

145 O. Tevet, P. Von-Huth, R. Popovitz-Biro, R. Rosentsveig, H.D. Wagner, and R. Tenne, *Proc. US Natl. Acad. Sci. USA*, 2011, **108**, 19901.

146 D. Maharaj and B. Bhushan, *Tribol. Lett.*, 2013, **49**, 323.

147 K.R. O'Neal, J.G. Cherian, A. Zak, R. Tenne, Z. Liu and J. L. Musfeldt, *NanoLett.,* 2016*, 16*, 993.

148 X.H. Wang, C.C. Zheng, and J.Q. Ning, *Sci. Rep.*, 2016, **6**, 33091.

149 M. Ghorbani-Asl, N. Zibouche, M. Wahiduzzaman, A.F. Oliveira, A. Kuc and T. Heine, *Sci. Rep., 2013,* **3**, 2961.

150 A. Nigues, A. Siria, P. Vincent, P. Poncharal, L. Bocquet, *Nat. Mat.*, 2014, **13**, 688.

151 J. Garel, I. Leven, C. Zhi, K.S. Nagapriya, R. Popovitz-Biro, D. Golberg, Y. Bando, O. Hod, and E. Joselevich, *Nano Lett.,* 2012*, 12*, 6347.

152 I. Leven, R. Guerra, A. Vanossi, E. Tosatti and O. Hod, *Nat. Nanotech.,* 2016*, 11*, 1082.

153 X.L. Wei, M.S. Wang, Y. Bando and D. Golberg, *Adv. Mater*, 2010, **22**, 4895.

154 R. Arenal, M.S. Wang, Z. Xu, A. Loiseau and D.Golberg, *Nanotech.*, 2011, **22**, 265704.

155 D.M. Tang, C.L. Ren, X. Wei, M.S. Wang, C. Liu, Y. Bando and D. Golberg, *ACS Nano*, 2011 5, 7362.

156 C. Zhi, Y. Bando, C. Tang, D. Golberg, *Mat Sci Eng R*, 2010 **70**, 92.

157 X. Chen, L. Zhang, C. Park, C.C. Fay, X. Wang and C. Ke, *Appl. Phys. Lett.*, 2015, **107**, 253105.

158 C. Yi, S. Bagchi, F. Gou, C.M. Dmuchowski, C. Park, C.C. Fay, H.B. Chew and C. Ke, *Nanotechnology*, 2018, **30**, 25706.

159 M. Antillon, P. Nautiyal, A. Loganathan, B. Boesl and A. Agarwal, *Adv. Eng. Mat.*, 2018, **20**, 1800122.

160 F. Xu, T. Kobayashi, Z. Yang, T. Sekine, H. Chang, N. Wang, Y. Xia, and Y. Zhu, *ACS Nano* 2017, **11**, 8114-8121.

161 A. Siria, P. Poncharal, A.L. Biance, R. Fulcrand, X. Blase, S.T. Purcell, L. Bocquet, *Nature,* 2013*, 494*, 455.

162 Y.J. Zhang, M. Onga, F. Qin, W. Shi, A. Zak, R. Tenne, J. Smet and Y. Iwasa, *2D Materials,* 2018, **5**, 035002.

163 T.V. Shubina, M. Remškar, V. Yu. Davydov, K.G. Belyaev, A. A. Toropov and B. Gil, *Ann. Phys.* (Berlin) 1800415 C (2019), DOI: 10.1002/andp.201800415.

164 D. R. Kazanov, A. V. Poshakinskiy, V. Yu. Davydov, A. N. Smirnov, I. A. Eliseyev, D. A. Kirilenko, M. Remskar, S. Fathipour, A. Mintairov, A. Seabaugh, B. Gil and T. V. Shubina, *Appl. Phys. Lett.* 2018, **113**, 101106.

165 A. Lavie, L. Yadgarov, L. Houben, R. Popovitz-Biro, T.-E. Shaul, A. Nagler, H. Suchowski and R. Tenne, *Nanotechnology*, 2017, **28**, 1361.

166 Y. Li, J.D. Cain, E.D. Hanson, A.A. Murthy, S. Hao, F. Shi, Q. Li, C. Wolverton, X. Chen, and V.P. Dravid, *Nano Lett*. 2016, **16**, 7696.

167 S. Fathipour, M. Remskar, A. Varlec, A. Ajoy, R. Yan, S. Vishwanath, S. Rouvimov, W.S. Hwang, H.G. Xing, D. Jena, and A. Seabaugh, *Appl. Phys. Lett.*, 2015, **106**, 022114.

168 R. Levi, O. Bitton, G. Leitus, R. Tenne and E. Joselevich, *NanoLett.,* 2013*, 13*, 3736.

169 Y. Divon, R. Levi, J. Garel, D. Golberg, R. Tenne, A. Ya'akobovitz and E. Joselevich, *NanoLett.*, 2017, **17**, 28.

170 F. Qin, T. Ideue, W. Shi, X.-X. Zhang, M. Yoshida, A. Zak, R. Tenne, T. Kikitsu, D. Inoue, D. Hashizume and Y. Iwasa, *Nano Lett.,* 2018*, 18*, 6789.

171 R. Arenal, O. Stephan, M. Kociak, D. Taverna, A. Loiseau and C. Colliex, *Physical Review Letters*, 2005, **95**, 127601.

172 L. Wirtz, A. Marini and A. Rubio, *Phys Rev Let*, 2006, **96**, 126104.

173 C.H. Park, C.D. Spataru and S.G. Louie, *Phys. Rev. Lett.*, 2006, **96**, 126105.

174 A. Pierret et al., *J. Appl. Phys.*, 2015, **118**, 234307.

175 X.G. Xu et al., *Nat. Comm.*, 2014, **5**, 4782.

176 J.-H. Jiang et al., *Opt. Express*, 2017, **25**, 25059.

177 B. Bhushan, B.K. Gupta, G.W. Van-Cleef, C. Capp, and J.V. Coe, *Trib. Trans.*, 1992, **34**, 573.

178 I. L. Singer, *in Fundamentals of Friction: Macroscopic and Microscopic Processes*, ed. I. L. Singer and H. M. Pollock, Kluwer, Dordrecht, 1992.

179 Y. Feldman, G.L. Frey, M. Homyonfer, V. Lyakhovitskaya, L. Margulis, H. Cohen, G. Hodes, J.L. Hutchison, and R. Tenne, *J. Am. Chem. Soc.,* 1996*, 118*, 5362-5367 (1996).

180 Drummond, C.; Alcantar, N.; Israelachvili, J.; Tenne, R.; Golan, Y., *Adv. Funct. Mater.*, 2001, **11**, 348.

181 M. Fojtů, W.Z. Teo and M. Pumera, *Environ. Sci. Nano* 2017, **4**, 1617.

182 X. Wu, X. Tian, T. Chen, A. Zeng and G. Yang, *Nanotechnology, 2018, 29*, 295604.

183 S.J. Panchu, S. Dhani, A. Chuturgoon and M.K. Moodley, *J. Photochem. & Photobiology, B: Biology,* 2018*, 187*, 10.

184 T. Zhang, T. Ma and W. Li, *J. Macromolecular Sci., Part B: Physics*, 2015, **54**, 992.

185 D.M. Simic, D.B. Stojanovic, S.J. Brzic, L. Totovski, P.S. Uskokovic b, Radoslav and R. Aleksic, Composites Part B, 2017, **123**, 10.